Twin boundary structure and mobility

Doron Shilo¹, Eilon Faran¹, Bibek Karki², Peter Müllner²

¹ Technion - Israel Institute of Technology, Haifa 3200003, Israel

² Boise State University, Boise, Idaho 83725, USA.

Corresponding Author: Eilon Faran, eilonfa@technion.ac.il, 972-54-8121123

Abstract

Twinning is an important mechanism of deformation in various crystalline materials, and in particular in shape memory alloys, where it is inherent to the shape memory and super-elasticity effects. This paper presents a generalized methodological approach for analyzing and modeling twin boundary dynamics with particular relevance for shape memory alloys. This approach combines the topological model description of the interface structure at the atomistic/lattice scale with analytical analysis of energy barriers and mechanisms of motion that provide macro-scale kinetic laws for the twin boundary motion. We emphasize the main differences between the topological structures of different types of twin interfaces and their implications for the mobilities of the different twin types. In particular, we elaborate on the relaxed topological structure of type II twin boundaries that contains a coherently facetted structure, where the facets are rational planes that accommodate misfit strain. Then, we clarify the lattice barriers' role in determining the different regimes of the kinetics of twin boundary motion. Further, we develop models leading to analytical expressions for the activation energies of various nucleation processes that dictate the overall kinetics of twin boundary motion, and identify of the rate-limiting process for the different twin types. In the case of compound and type I twins, the analysis leads to an explicit expression for the magnitude of the twinning stress, revealing a strong dependency on the shear modulus and the twinning shear, which is in excellent quantitative agreement with experimental values reported for different materials. Moreover, our analysis reasons the different temperature dependencies of the twinning stress exhibited by the different twin types, and in particular the very low temperature sensitivity of type II twins.

1. Introduction

Twinning is an essential mode of plastic deformation in a variety of solid materials, such as hexagonal close-packed (HCP) metals (e.g., Mg and Ti) [1], nano-crystalline and nano-structures of face-centered cubic (FCC) metals (e.g., Cu and Ni) [2–4]. Besides, twinning reorientation in ferroelectric materials and shape memory alloys (SMA) facilitates significant straining [5], thus providing the fundamental mechanisms for transformation between electric/magnetic/thermal energy and mechanical energy, which are used in a variety of advanced actuation, sensing, and energy harvesting applications [6–9].

Given the importance of twinning to the functionality of advanced materials, an understanding of interrelations between the often-complex twin boundary (TB) structure of different twin types and their mobility is required. Further, the knowledge of the relations between twin boundary mobility and fundamental material properties, such as the twinning shear strain and the shear modulus, is of substantial importance. Such knowledge can be acquired through the development of general yet simple microstructure-based models, that can be applied to different material systems (see, e.g., Refs. [10,11]). This approach should be validated by its power to explain twinning behavior based on fundamental material properties such as lattice parameters, twinning elements, and elastic constants, and on experimental evidences that have been reported in recent years.

In the classical description of twinning, twins are related by a simple shear. The classical model predicts the twinning mode of a given crystal lattice by identifying the twinning elements: the twinning invariant planes K_1 , K_2 , the twinning directions η_1 , η_2 , and the twinning shear strain s [1,12–14]. Following this description, twins are classified into three types: type I, type II and compound. In type I twins, K_1 and η_2 are rational, while K_2 , η_1 are irrational. In type II twins K_1 and η_2 irrational while K_2 , η_1 are rational. In compound twins, all four twinning elements are rational. In tetragonal martensite (e.g., BaTiO₃ [15], non-modulated Ni-Mn-Ga [16]) only compound twins exist, while all three twin types can exist in lower symmetry structures, such as monoclinic (e.g., NiTi [17], 10M Ni-Mn-Ga [18]) and rhombohedral and hexagonal (e.g., Cu-Al-Ni [19], Ti-Al [20]) martensite.

Experiments indicate that the dynamics of type II twins are fundamentally different from those of type I twins. Type II twins display smaller twinning stress values than type I, as reported for several material systems, e.g., Ni-Mn-Ga, Ni-Mn-Sn, and Cu-Al-Ni [18,19,21]. For these materials, the room temperature twinning stress of type II twins is smaller than that of the conjugate type I twins by at least a factor of 5 [18,22,23]. Previous studies by several research groups, focusing mainly on the Ni-Mn-Ga system, have attempted to explain these differences based on the complex twinned microstructure occurring at various length scales [24–29]. Here, we analyze and explain the different mobilities of type I and II twins based on the periodicity of the lattice as a source for energy barriers and the different lattice-scale topological structures.

Moreover, the twinning stress of type II twins shows a very weak, in some cases undiscernible, temperature sensitivity (e.g., Ni-Mn-Ga, Cu-Al-Ni [30–32]). This is in contrast to the behavior of type I and compound twins, which typically display an increase in twinning stress as the temperature is decreased relative to the martensite to austenite transformation temperature [21,32–34]. Such behavior indicates that the rate-limiting process in the motion of type II twins is different from that in compound and type I twins. Moreover, a finite and relatively low twinning stress value of type II TB was reported for 10M Ni-Mn-Ga at temperatures as low as 1.7 K [30]. This indicates that the mechanisms responsible for TB motion can proceed in an athermal manner even at low driving force values.

The evolution of twinning, i.e., the micro mechanisms and kinetics by which one twin expands at the expense of another through the motion of twin boundaries (TBs), is associated with the nucleation and propagation of twinning defects known as twinning disconnections (TD). A disconnection is a linear defect with both step and dislocation characters [35,36]. Therefore, a thorough understanding of the origin and dynamics of twinning requires the knowledge and modeling of the defect structure and the corresponding physical mechanisms of motion.

The content, properties, and arrangement of TBs and TDs can be well described with the topological model (TM) [35–38]. Researchers have applied the TM to explain the formation and motion of many interfaces, including precipitate/matrix interfaces, martensite/austenite interfaces, as well as compound and type I twins [1,38,39]. Type II twins, which play a dominant role in twinning evolution in many SMA, pose a challenge for the TM description because of the irrational character of their twinning plane that results in an undefined distance between consecutive twinning planes. Recently, Pond et al. introduced a TM-based description for the formation of type

II twins and implemented it to several material systems (e.g., α – Ur, NiTi) [40,41]. Following these works, possible equilibrium structures of type II twins in Ni-Mn-Ga and Ni-Ti were proposed based on the TM [42,43]. Sehitoglu et al. [44] used a combined atomistic-topological approach to describe an equilibrium structure of type II twins in Ni-Ti.

The TM provides a crucial bridge between TB structure and mobility, as it describes the twinned interface as an arrangement of TD defects whose nucleation and motion can be evaluated based on principles of the classical dislocation theory. Specifically, the mobility of a TD is directly related to the fundamental properties of the linear defect: the burgers vector \boldsymbol{b} and the core width δ , and potentially other interfacial properties, such as the step height \boldsymbol{h} . For example, small burgers vector and large core width are expected to promote high mobility of a linear defect. A fundamental feature of any twinning system is the twinning shear strain \boldsymbol{s} . The TM indicates that the magnitude of \boldsymbol{s} is related to the properties of a TD according to $\boldsymbol{s} = \boldsymbol{b}/\boldsymbol{h}$ [36]. Different materials, as well as different twinning systems within the same material, have significantly different twinning shear values [1]. In these cases, the twinning shear may strongly influence the twin boundary mobility.

In this study we analyze the impact of topological parameters on the mobility of twin boundaries. The topological parameters derive from the crystal structure and orientation. To facilitate the crystallographic representation of twinning for modulated martensite in different SMA, the TM adopts an approximated crystallographic structure that averages out the modulation. (e.g., an effective monoclinic unit cell in 10M Ni-Mn-Ga, Refs [42,45]). This approach is useful for defining and quantifying the topological parameters of the interface defects (e.g., b,h). In addition, it allows describing the lattice barrier for TB motion (see section 4) by a simple periodic function with periodicity on the order of a single lattice spacing of the effective unit cell. By averaging out the lattice modulation we disregard shuffles required to establish the correct structure. In the cases discussed here, particularly for type II twins in 10M Ni-Mn-Ga, shuffles are very small (substantially below the interatomic distance) and do not include the switching of atoms. In such cases, shuffle does not contribute significantly to twin boundary mobility [1].

In order to establish general relations between the structure of the TB (as described by the TM) and its mobility, the mechanisms of motions for twins in various materials must be clarified. In this context, a mechanism of motion is a description of a sequence of several sub-processes by which the TB propagates and an identification of the rate-limiting process. This knowledge allows the formulation of kinetic relations that quantify the velocity of the interface as a function of the

thermodynamic driving force. The term driving force represents the sum of all tractions that act on a twin boundary through various types of external loads (e.g., mechanical, magnetic, electrical), as further explained in Section 2. The kinetic relation is the basic input for models describing the macroscopic mechanical response of materials due to twinning.

Recently, Müllner analyzed the mechanisms of motions associated with nucleation of new TDs, focusing on the relations between the TM of type I and II boundaries and the resulting barriers for TD nucleation [11]. Faran and Shilo suggested analytical models for the kinetic relations of TB motion, based on different mechanisms of motion [46,47,23]. These studies revealed a clear transition between slow and fast regimes of motion that takes place at driving forces much larger than the value related to the twinning stress [46–49]. The source for this transition is not yet fully explained. Specifically, it is unclear if this source is different for type I and II twin boundaries and is this transition expected to appear in other SMA.

This paper is organized as follows: section 2 presents several basic concepts that are essential for the analysis of TB motion in a variety of material systems, focusing on the definitions and application of the driving force and kinetic relations. Section 3 contains a basic description of the structure of a twinning interface based on the TM. In section 4 we present the energy barriers that are imposed by the lattice and resist the motion of the TB, which leads to the classification of different regimes of the twin boundary motion. Section 5 presents an analytical formulation of the activation energies of different processes that occur during the twin boundary motion. In section 6 we focus our analysis on TB motion in the slow rate regime and identify the rate limiting process that determines the dynamics of different twin types. Further, we obtain explicit expressions for the twinning stress for the driving force regime where thermal activation dominates the kinetic relation and for the different nucleation energies that were developed in section 5. In section 7 we employ the insights presented in the previous sections and reason the available results for the motion of different twin types in different materials systems. Emphasis is given to results reported on ferromagnetic SMA 10M Ni-Mn-Ga because TB motion in this system was widely investigated by several research groups with high quality single crystals.

2. Definitions and basic concepts

Commented [CU1]: I am not sure if this is correct though "thermally activated kinetic relation" is incorrect. The relation is not thermally activated.

When discussing the motion of TB, several basic concepts should be defined and clarified to allow for a general description that is valid for a variety of material systems. We start with the concept of the *thermodynamic driving force* (*driving force* in short) g, which is well known from the field of phase transformations, and represents the change in free energy due to the transformation from one state (or phase) to another [50–52]. For the case of a TB, the *driving force* is the derivative of the TB energy \overline{U}_{TB} (per unit area) with respect to the propagation coordinate z normal to the TB plane:

$$g = -\frac{\partial}{\partial z} \left(\overline{U}_{TB} \right) \tag{1}$$

The driving force has the dimension of energy per volume. Eq. (1) represents a continuum (macroscopic) model, and the definition of \overline{U}_{TB} does not account for local atomistic effects such as the lattice potentials. The influence of the lattice periodicity on the TB energy is introduced in section 4. A similar expression can be formulated for the case of a linear TD defect [53,54].

The total energy \overline{U}_{TB} contains several contributions, which represent the strain, electric (e.g., in ferroelectric crystals), and magnetic (e.g., in ferromagnetic crystals) energies that vary due to the TB propagation:

$$\overline{U}_{TB} = U_{TB}^{mech} + U_{TB}^{elec} + U_{TB}^{mag} \tag{2}$$

The use of the *driving force* is general and allows us to decouple the thermodynamic traction applied on a moving material defect from the overall mechanical state of the macroscopic crystal. For example, Eq. (1) and (2) show that a ferromagnetic crystal subjected to external magnetic field results in a non-zero driving force for TB motion, even if there is no mechanical load. In this case, the frequent use of the term *magneto stress*, which is equivalent to the effect of the magnetic driving force (U_{TB}^{mag} in Eq. (2)), is ambiguous since it is not a real mechanical stress and does not appear in the basic equations of force equilibrium over the macroscopic crystal. Furthermore, the general formulation of the *driving force* enables accounting for other effects, such as that of demagnetization energy (as in Refs. [47,55]) or cases where the TB area is not constant.

The kinetic relation [51,56] is a constitutive material law that correlates the velocity of an individual TB to the thermodynamic driving force. Different kinetic relations may arise for different ranges of the driving force, but all kinetic relations are determined by properties at the atomistic and mesoscopic scales. Kinetic relations serve as the basic input in models describing the overall twinning dynamics. Specifically, discrete twin boundary dynamic simulations, based on measured kinetic relations, have been demonstrated as a powerful tool for calculating the dynamic response of Ni-Mn-Ga actuators [57,58]. Kinetic relations can be obtained experimentally by tracking the motion of individual TBs [46,47], and can also be formulated analytically. To the latter end, one must identify the mechanism of motion and formulate the kinetic laws for the rate of this mechanism. Comparing experimental and analytical kinetic relations allows validating the assumptions taken during the analytical approach and extracting values of basic material properties [23,47].

Another common term in the dynamics of twinning is the *twinning stress*, which is usually obtained from quasi-static uniaxial mechanical experiments at strain rates typically slower than $10^{-2} \, s^{-1}$ [59]. Under these conditions, the only non-zero term in Eq. (2) is the mechanical energy, $U_{TB}^{mech} = -z \cdot \sigma_{TS} \cdot \varepsilon_S$. Here, σ_{TS} is the twinning stress, which is typically measured along a <100> longitudinal direction of a single crystal cut with faces parallel to {100} planes of the parent cubic phase (e.g., Refs. [60,19,61,21]). ε_S is the corresponding longitudinal strain (i.e., along the same direction as σ_{TS}) associated with TB motion. For example, $\varepsilon_S = 1 - c/a$ in tetragonal martensite. z is the propagation distance normal to the TB plane, to straddle a volume that is transformed due to the TB motion. Since the twinning shear equals $s = 2\varepsilon_S$, the specific driving force g_{TS} (energy / volume, Eq. (1)) associated with the twinning stress is given by:

$$g_{TS} = \frac{\sigma_{TS} \cdot s}{2} \tag{3}$$

In cases where the mechanism of motion is thermally activated, the *twinning stress* σ_{TS} depends on the temperature and the applied strain rate (or TB velocity). Therefore, in general, the *twinning stress* is not identical to a barrier for the twin boundary motion.

3. Topological models for twin interfaces

While the classical description of twinning predicts the twinning mode of a given lattice (see section 1), this model does not clarify the micro mechanisms of twinning. For instance, it does not provide insight into the formation mechanism and equilibrium structure of type II twin because the invariant plane K_1 is irrational in this case [1]. The topological model proposed by Pond and Hirth [36,37,39,40,62] provides a framework to extensively characterize the defect contents of interfaces, including twinning [63,64]. The model assumes the formation and growth of terraces separated by disconnections as the mechanism of formation and growth of twins.

In compound and type I twins, the invariant plane of twinning, K_1 , is rational, and thus disconnections, (b,h), are intuitively defined in the interface [37]. For example, for a type I twin, the Burgers vector, b, of the disconnection is parallel/antiparallel to the shear direction, η_1 , and the step height, h, is equal to the interplanar spacing of the K_1 plane. The Burgers vector quantifies the lattice displacement required for maintaining a coherent interface, and the step height quantifies the displacement of the interface accompanying the motion of the disconnection. In a relaxed condition, the lowest energy configuration of a TB is a flat K_1 plane without any disconnections.

The twinning plane of type II twins is irrational, which poses intuitive (but not conceptual) difficulties in describing the topological structure of the interface. This has motivated several studies, both theoretical [40–42,44] and experimental [65–69] in an attempt to unravel the equilibrium structure of a type II interface. These studies state that an irrational twinning plane possesses high energy, which promotes relaxation of the interface to various types of lower energy configurations. For example, experimental characterization using HRTEM images sometimes reveals a faceted structure [68,69], while in other cases, the structure relaxes more randomly [65]. Macroscopically, the orientation of the relaxed twinning plane coincides with the irrational plane predicted by the classical theory of twinning.

A flat twinning plane that lays along an irrational crystallographic plane is highly incoherent, since the two twins only share a common lattice direction but not a plane. The incoherency results in a high interfacial energy, and thus the atomistic structure of the type II TB is likely to relax to lower energy configurations [70]. A possible relaxed interface for type II TB is the formation of a

Commented [Bk2]: They share a rational direction (η_1) , but not a lattice plane.

coherently faceted structure [71,68,44,42]. In this description (**Fig. 1**), the TB forms facets that lie along low-index planes, separated by equally spaced steps that lie along another low-index plane. The "average" interface plane, formed by the facets and the steps, lies very close to the irrational twinning plane K_1 , calculated based on the classical theory of twinning. In general, while the low-index facet planes are common to both the parent and the twin, there is some in-plane rotation of the lattices of the parent and the twin within this plane. This rotation results in a misfit of the parent and twin lattices in the facet plane. This misfit can be accommodated either by long range elastic strains, resulting in a fully-coherent interface, or by an array of misfit screw dislocations, resulting in a coherently faceted interface. For some materials, e.g., Ni-Ti, the misfit screw dislocations coincide with the steps between facets, as demonstrated in **Fig. 1**, thus forming an array of equally spaced misfit screw disconnections, characterized by a step height and a Burgers vector [44]. In other materials, such as Ni-Mn-Ga, the direction of the Burgers vector of the misfit dislocation results in steps that rotate the average plane formed by the faceted interface out of the irrational K_1 plane [42]. Thus, for these materials, the description of the twin boundary as a coherently faceted structure is still an unsolved problem.

At a scale larger than the equilibrium distance between adjacent disconnections (l_0 in Fig. 1), which is on the order of few nm (Refs. [42,44] and values in Table 2), the strain field produced by the array of dislocations is equal in magnitude but opposite in sign to the strain field produced by the misfit at the faceted interfaces. Thus, the two contributions cancel each other, resulting in zero long-range strains. In materials where the coherently faceted structure is possible, the array of equally spaced disconnections represents a low-energy configuration of the type II TB, and can thus serve as an equilibrium state.

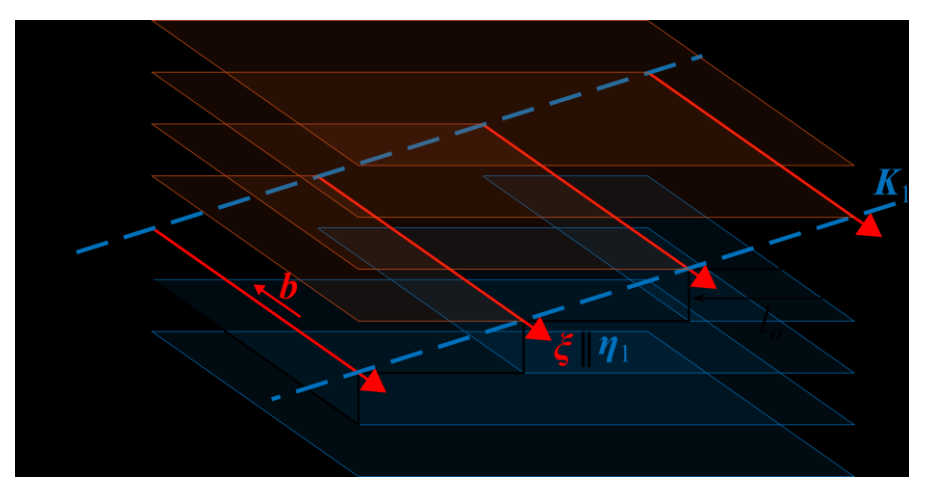


Fig. 1 Schematic illustration of a coherently faceted type II TB, showing the low index plane facets separated by an array of screw disconnections. b is the Burgers vector of a disconnection, ξ is the disconnection line direction and is (anti) parallel to the shear direction η_1 . The disconnections are equally spaced at a distance l_0 , such that the average interface plane coincides with the irrational K_1 twinning plane.

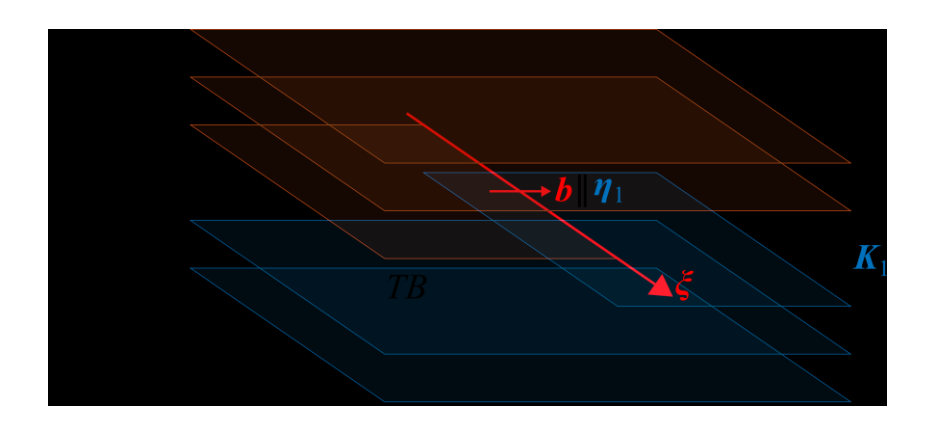
4. Lattice barriers for twin boundary motion and classification of different regimes

To define possible mechanisms of motion that lead to twin boundary propagation, we identify the energy barriers that resist each sub-process involved in the motion. Here, we present a general analysis that considers only the periodicity of the lattice as a source for energy barriers. Other, aperiodic barriers may arise due to interactions of the twin boundary with crystal defects, such as surface roughness, precipitates, dislocations, phase boundaries, and grain boundaries. The effects of these barriers depend on the specific problem and the quality of the crystal. The lattice barriers are shown in Fig. 2 and the different sub-processes are summarized in Table 1. Two different barriers separate the driving force scale into three regions. In each of these regions, different processes take place, resulting in different velocities through different kinetic relations.

Compound and type I TB's are parallel to low-index lattice planes. Such interfaces are subjected to a lattice barrier that resists their motion as a flat plane. The periodicity of this barrier is equivalent to the lattice spacing of the low-index plane, d_{TB} , and its amplitude is denoted as γ_{TB}

(energy per unit area), as shown in **Fig. 2**(a). Type II twin boundaries, on the other hand, are characterized by an irrational twinning plane, which poses difficulties in realizing the role of a periodic lattice barrier that resists the propagation of the twin boundary as a flat plane. However, we note that the step height of disconnection on a type II interface has a discrete value. For Ni-Mn-Ga, the step height is of the same order of magnitude as d_{TB} [42]. Moreover, the coherent facets that constitute the coherently faceted structure lay on low index planes (**Fig. 1** and related discussion), and are thus subjected to a periodic lattice barrier.

An additional periodic lattice barrier is associated with the motion of twinning disconnections. A disconnection line tends to lay along low-index lattice directions, even when the burgers vector is irrational, e.g., in type I twins [42], and is thus subjected to a periodic lattice barrier that resists its glide, similarly to the Peierls barrier for the glide of ordinary dislocations. The periodicity of the Peierls barrier is the lattice spacing perpendicular to the disconnection line on the glide plane, d_D , and its amplitude is denoted as Γ_D (energy per unit length), as shown in **Fig. 2**(b).



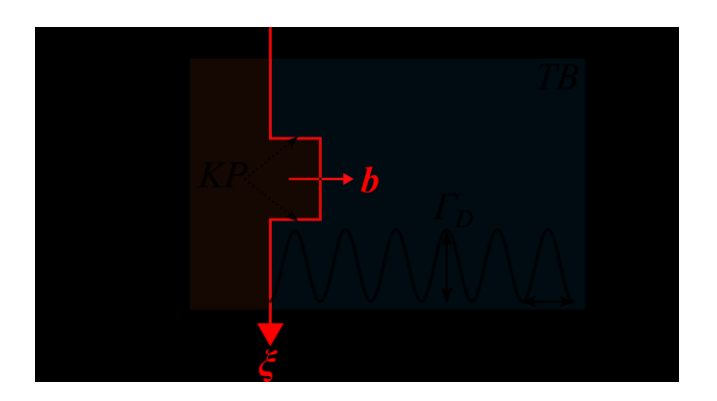
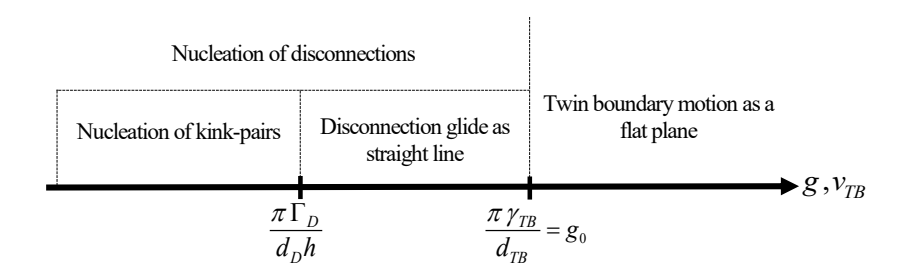


Fig. 2 Schematic description of the different lattice barriers for TB motion. The illustrations depict a TB with a rational twinning plane K_1 , as in compound and type I twins. (a) The lattice barrier for the motion of the TB as a flat plane along z direction. The barrier is characterized by an amplitude γ_{TB} (energy/area) and periodicity d_{TB} . The TB can also propagate via the glide of twinning disconnections on the rational twinning plane K_1 , along x direction. b, ξ are the Burgers vector and line direction of the disconnection, and η_1 is the shear direction. (b) Peierls barrier for the glide of a disconnection. The barrier is characterized by an amplitude Γ_D (energy/length) and periodicity d_D . A kink-pair (KP) mechanism allows disconnection motion at driving force values that are smaller than the Peierls barrier.

Table 1: Sub-processes in the various ranges of the driving force (g) and TB velocity (v_{TB}). The different ranges of the driving force are defined based on the magnitudes of the lattice barriers Γ_D , γ_{TB} .



To evaluate the effects of the lattice barriers presented in **Fig. 2** on the motion of a TB, we introduce periodic functions that depict the energy landscapes of the lattice barriers, and add them to the total energy of the system. In **Fig. 3** and **Fig. 4** we plot the energy landscapes encountered by a moving TB and a moving TD, for two ranges of the external driving force with respect to the lattice barrier amplitude. This representation corresponds to cases where the driving force is the input parameter and dictates the dynamics of the TB or TD through fundamental kinetic relations (see, e.g., Refs. [47,48]). The analysis presented below shows that the energy landscapes are qualitatively similar for a moving TB and a TD, and thus the schematic plots in **Fig. 3** and **Fig. 4** are valid to both defect types.

For an existing TB, we express the change in energy per unit area U_{TB} , as a function of the boundary position z, where z is the coordinate perpendicular to the boundary plane (Fig. 2(a)):

$$U_{TB}(z) = -gz + \gamma_{TB}\sin^2\left(\frac{\pi z}{d_{TB}}\right) \tag{4}$$

The first term in Eq. (4) is the work per unit area associated with the motion of the TB under the driving force g along the coordinate z (identical to the continuum quantity $\overline{U}_{TB}(z)$ in Eq. (1)). The second term in Eq. (4) represents the periodic lattice barrier for TB motion (Fig. 2a). Analysis of Eq. (4) points to two different cases. In the driving force range $g > g_0$, where $g_0 = \frac{\pi \gamma_{TB}}{d_{TB}}$ is the driving force associated with overcoming the lattice barrier γ_{TB} , the function $U_{TB}(z)$ decreases monotonically for all values of z (Fig. 3). In this case, the driving force enables overcoming the lattice barrier, and the twin boundary moves as a flat plane. In this regime, the twin boundary motion is restricted only by the internal friction of the material and does not require a thermally activated process.

If
$$g < \frac{\pi \gamma_{TB}}{d_{TB}}$$
 the twin boundary encounters a positive energy barrier (marked as U_{TB}^{bar} in **Fig. 4**)

as it propagates from one potential well to the next. Therefore, motion in this range of the driving force necessitates nucleation of disconnections and their further glide. This motion type results in a slower advancement of the TB than the motion as a flat plane. For compound and type I twins,

whose equilibrium topological structure does not contain disconnections, the nucleation requires overcoming an energy barrier via a thermally activated process, as discussed in section 5.2. For type II twins, where disconnections are an inherent part of the equilibrium structure, there is a unique mechanism of athermal heterogeneous nucleation of disconnections at the surface, as we discuss in detail in section 5.3.

A similar analysis is applicable also for the motion of a disconnection. The change in energy (per unit length) of the disconnection is given by

$$u_D(x) = -ghx + \Gamma_D \sin^2\left(\frac{\pi x}{d_D}\right)$$
 (5).

Here -ghx is the work per unit length associated with the motion of the disconnection along a distance x under the driving force g, x is the coordinate perpendicular to the disconnection line on the twinning plane (**Fig. 2**(b)), and h is the step height of the disconnection. The second term in Eq. (5), represents the periodic lattice barrier for disconnection motion (**Fig. 2**(b)).

When $g > \frac{\pi \Gamma_D}{d_D h}$ in Eq. (5), the function $u_D(x)$ decreases monotonically for all values of x

(Fig. 3) and the disconnection can propagate as a straight line in an athermal manner and its motion is restricted only by the internal viscosity (i.e., does not require a thermally activated process).

Alternatively, when $g < \frac{\pi \Gamma_D}{d_D h}$, the disconnection encounters a positive energy barrier, u_D^{bar} , as it

propagates from one potential well to the next (**Fig. 4**). Following classical dislocation theory (see, e.g., p. 242 in Ref. [72]), motion of a disconnection in this range of the driving force is possible through nucleation of kink pairs on the disconnection line and the subsequent expansion of the kinks along the disconnection line (**Fig. 2**(b)). The kink pair mechanism for the advancement of a TB is reproduced in atomistic simulations of twinning in ferroelastics (see. e.g., Ref. [73]).

The above discussion implies that under any value of the driving force there exists a mechanism of motion that can lead to the propagation of the TB, as summarized Table 1. In practice, the actual movement mechanism of the TB may be indistinguishable in a specific type of experiment. For example, slow-rate mechanical tests apply a constant controlled strain rate on the sample. The stress reaches a plateau, denoted as the twinning stress, at a value at which the microscopic strain

rate induced by the moving twin boundary is equal to the macroscopic strain rate. At stress levels smaller than the twinning stress, the stress increases, but this does not mean that there is no twin boundary motion in this range.

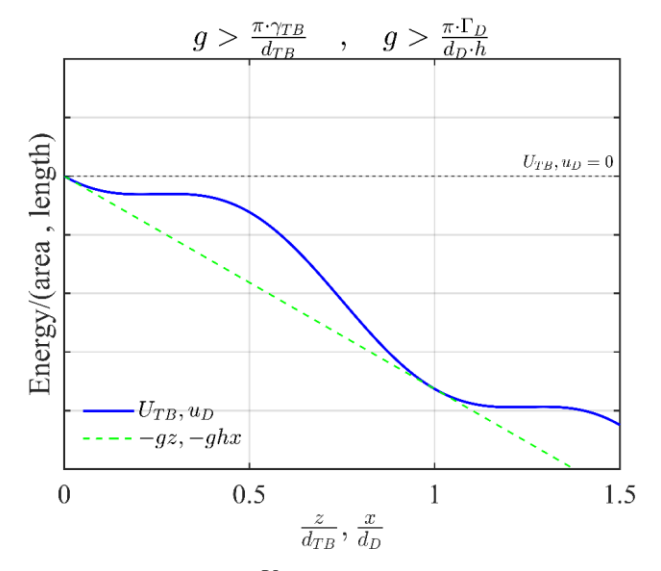


Fig. 3 Energy profile of a twin boundary U_{TB} (energy/area, Eq.(4)) or twinning disconnection u_D (energy / length , Eq. (5)), for the case that the driving force g (energy/volume) is larger than the lattice barrier. The dashed green line represents the work associated with the motion of the TB (-gz in Eq.(4)) or the disconnection (-ghx in Eq. (5)). The normalized coordinates z/d_{TB} , x/d_D represent the directions normal to the TB plane and disconnection line, respectively (as in Fig. 2).

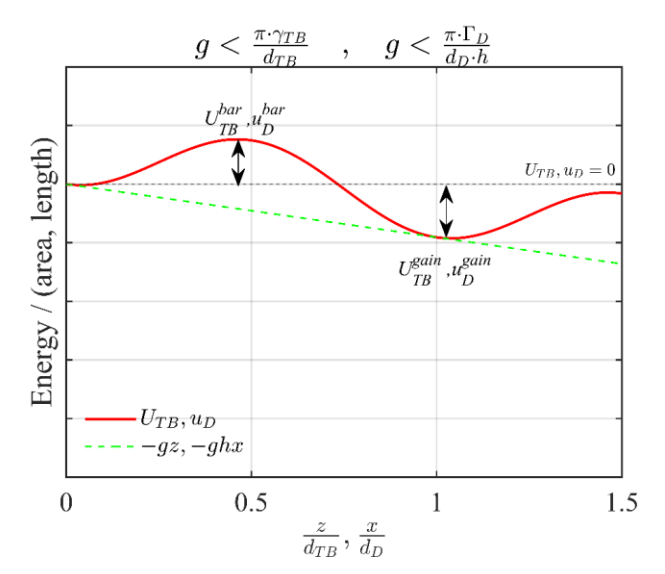


Fig. 4 Energy profile of a twin boundary U_{TB} (energy/area, Eq.(4)) or twinning disconnection u_D (energy/length, Eq. (5)), for the case that the driving force g (energy /volume) is smaller than the lattice barrier. The dashed green line represents the work associated with the motion of the TB (-gz in Eq.(4)) or the disconnection (-ghx in Eq. (5)). The normalized coordinates z/d_{TB} , x/d_D represent the directions normal to the TB plane and TD line, respectively (as in Fig. 2). The magnitude of the barrier for TB or disconnection motion associated with the lattice potential is marked as U_{TB}^{bar} and u_D^{bar} , respectively. The energy gained due to the local advancement of the TB or the disconnection is labeled as U_{TB}^{gain} and u_D^{gain} , respectively (see discussion on the different energy terms in sections 5.1 and 5.2).

5. Activation energies for nucleation processes

In section 4 we identified two nucleation processes associated with different mechanism of TB motion, namely the nucleation of disconnections and the nucleation of kink pairs on disconnections. Next, we formulate analytical expressions for the corresponding activation energies of these nucleation processes, and discuss their relevance to the motion of the different type of TB's. Here, we distinguish three nucleation processes: the first analyzes the nucleation of kink-pairs on an existing disconnection line. This mechanism is required for the glide of a disconnection and thus, it is applicable to all twin types. The second process is the homogenous nucleation of disconnection loops that is relevant mainly to compound and type I twins. The third

process is the heterogenous nucleation of disconnections at the surface that is unique to the relaxed structure of type II twins.

In the following analysis, we employ isotropic elasticity for evaluating the energies of individual disconnections and disconnection arrays. This provides simple analytical expressions that can be quantified and compared between different material systems. Yet, isotropic elasticity assumes that the shear stiffness is identical in all directions, which is not the case for elastically anisotropic martensitic SMA. In order to account for this, we associate the shear stiffness μ in the isotropic formulation with the C' elastic modulus of the austenite phase near the martensitic transformation temperature, and not with the isotropic shear modulus G (see values in Table 2, Table 3, and similar discussion in Ref. [11]).

5.1 Homogeneous nucleation of kink pairs on disconnection lines.

When the driving force is smaller than the Peierls barrier for disconnection glide (i.e., $g < \frac{\pi \Gamma_D}{d_D h}$

), the glide of a disconnection requires the nucleation and expansion of kinks. This allows part of the disconnection to locally overcome the energy barrier u_D^{bar} , as illustrated in Fig. 4. Based on the theory of dislocation kinks (Ref. [72], page 242), we consider the homogenous nucleation of a kink-pair on an existing disconnection line.

The activation energy for the homogenous nucleation of a kink-pair with a kink separation y is expressed by:

$$Q_{KP} = u_D^{bar} \cdot y + E_{KP}^{self} \left(y \right) \tag{6}$$

Here, u_D^{bar} is the energy per unit length required to overcome the periodic Peierls potential of the disconnection, and is equal to the first maximum of the disconnection energy $u_D(x)$ (given by Eq. (5).), calculated at $x = d_D/2$ (see Fig. 4):

$$u_D^{bar} = u_D \left(x = d / 2 \right) = \Gamma_D - g \cdot h \cdot \frac{d_D}{2}$$
 (7)

 $E_{KP}^{self}(y)$ in Eq. (6) is the self-energy of the kink-pair and is generally given by:

$$E_{KP}^{self} = 2e_f - \frac{e_{\text{int}}}{v} \tag{8},$$

where, e_f and e_{int} are formation and interaction energies, respectively. Under the approximation of isotropic elasticity, the two energies scale as $e_f \square$ and $e_{\text{int}} \square$ (see Ref. [72], page 244), where μ is the shear stiffness.

Both terms in Eq. (6) are positive and increase as y increases. Further, after the nucleation, if y is too small, the attraction forces between the two kinks results in an annihilation of the kinks. Therefore, we must find the minimal value of y for which the nucleated kink-pair tends to grow, i.e., to increase the value of y. For this purpose, we express the energy of an existing kink-pair, for which $x = d_D$, as a function of y:

$$E_{KP}^{\text{existing}}\left(x=d_{D}\right) = u_{D}^{\text{gain}}y + E_{KP}^{\text{self}}\left(y\right) = -g \cdot h \cdot d_{D} \cdot y + E_{KP}^{\text{self}}\left(y\right) \tag{9}$$

Here, u_D^{gain} is the first minima of the energy of the disconnection u_D (Fig. 4). At $x = d_D$ the periodic lattice barrier (2nd term in Eq. (5)) is zero, and thus:

$$u_D^{gain}(x=d_D) = -g \cdot h \cdot d_D \tag{10}$$

The critical length of the kink pair y_c is obtained by finding the first extremum of Eq (9), i.e., solving $\frac{\partial E_{KP}^{existing}}{\partial y} = 0$, which provides:

$$y_c = \sqrt{\frac{e_{\text{int}}}{g \cdot h \cdot d_D}} \tag{11}$$

And thus, Eq. (6) becomes:

$$Q_{_{KP}} = \left(\Gamma_{_D} - g \cdot h \cdot \frac{d_{_D}}{2}\right) y_c + \left(2e_f - \frac{e_{_{int}}}{y_c}\right)$$
(12)

Under the conditions of thermally activated motion (i.e., $g < \frac{\pi \Gamma_D}{d_D h}$), both bracketed terms in Eq. (12) are positive, and thus the total activation energy Q_{KP} is always positive. This implies that kink-pair nucleation is not a spontaneous process, and requires some finite activation energy. As we show in section 7.3, in some twin types and material systems the magnitude of Q_{KP} is comparable to the thermal energy even near 0 K temperature. Thus, a finite concentration of kinks is expected to be always present on the disconnection line even under zero driving force (see also Ref. [74]). At the same time, TB motion requires annihilation of existing kinks and nucleation of fresh kink-pairs. The rate of the later process is determined by the driving force g.

5.2 Thermally activated homogeneous nucleation of disconnection loops

In compound and type I twins, the equilibrium structure of the twin boundary is a flat interface that coincides with a low index plane. Thus, when the driving force is lower than the barrier for twin boundary motion as a flat plane, i.e., $g < \frac{\pi \gamma_{TB}}{d_{TB}}$, twin boundary motion requires the nucleation of disconnections on the TB plane. We consider nucleation of disconnection loops in the bulk or nucleation of half-loops at the surface, under the application of an external driving force g. This

nucleation process is consistent with the recent description of an evolving topology of type I and compound twins under non-zero loading conditions (see Ref. [75]).

The analytical approach is similar to that employed for the nucleation of kink-pairs, in section 5.1. The activation energy for the nucleation of a disconnection loop with a radius r is expressed by:

$$Q_{DL} = U_{TR}^{bar} \cdot \pi r^2 + E_{DL}^{self}(r) \tag{13}$$

The first term on righ-hand side of Eq. (13), $U_{TB}^{bar} \cdot \pi r^2$, represents the energy required to move the disconnection loop across the lattice barrier perpendicular to the twinning plane under the application of an external driving force g (Fig. 4 and also in Ref. [47]). The magnitude of the barrier (energy per unit length) is given by

$$U_{TB}^{bar} = \gamma_{TB} - g \cdot \frac{d_{TB}}{2} = d_{TB} \left(\frac{g_0}{\pi} - \frac{g}{2} \right)$$
 (14)

Where we substituted $\gamma_{TB} = \frac{d_{TB}g_0}{\pi}$.

The barrier U_{TB}^{bar} is positive within the relevant range of the driving force $g < \frac{\pi \gamma_{TB}}{d_{TB}}$. The second term in Eq. (13) $E_{DL}^{self}(r)$ represents the self-energy of the disconnection loop. The magnitude of $E_{DL}^{self}(r)$ may depend on the type of nucleation process. Heterogeneous nucleation of a disconnection loop, for example at crystal defects, may result in negligibly small value of $E_{DL}^{self}(r)$. This in turn, may lead to a negligibly small activation energy Q_{DL} . However, given that the equilibrium structure of compound and type I twins contains no disconnections, continuous motion of the TB at a scale larger than the lattice scale requires nucleation events that occur regardless of the TB position within the crystal, i.e., not just in some few specific locations of crystal defects. Thus, we consider here the case of a homogenous nucleation, for which the activation energy given by Eq. (13) is always positive and increases as r increases.

After the nucleation event, if r is too small, the attraction forces between segments of the disconnection loop will result in an annihilation of the loop. Therefore, we find the minimal value of r for which the nucleated disconnection loop tends to grow, i.e., to increase the value of r. For this purpose, we express the energy of an existing disconnection loop with radius r:

$$E_{DL}^{\text{existing}}\left(r\right) = U_{TB}^{\text{gain}} \pi r^2 + E_{DL}^{\text{self}}\left(r\right) \tag{15}$$

Eq. (15) describes the energy of a loop that has already "surpassed" the activation energy Q_{DL} (expressed in Eq. (13)). Thus, $U_{TB}^{gain} \equiv U_{TB} \left(z = d_{TB}\right)$ represents the first minima of U_{TB} and it has a negative value (see Eq. (4) and **Fig. 4** in section 4). This distinguishes Eq. (15) from Eq. (13), where U_{TB}^{bar} represents the first maxima of U_{TB} , and it has a positive value. Further, the lattice potential (second term in Eq. (4)) is zero at $z = d_{TB}$. Thus, Eq. (15) becomes:

$$E_{DI}^{existing}(r) = -gd_{TR} \cdot \pi r^2 + E_{DI}^{self}(r)$$
(16)

The self-energy of the disconnection loop $E_{DL}^{self}(r)$ can be expressed using the energy per unit length of the disconnection loop, $q_D(r)$:

$$E_{DL}^{self}(r) = 2\pi r \cdot q_D(r) \tag{17},$$

Equation (16) has a maximal value at $r=r_c$. For $r < r_c$, $\partial E_{DL}^{exsiting}/\partial r > 0$, which means that such a loop will collapse and disappear. For $r > r_c$, $\partial E_{DL}^{exsiting}/\partial r < 0$, which means that such a nucleated loop will grow and increase its radius. Thus, only loops with $r > r_c$ contribute to the propagation of the twin boundary. For loops with $r \ge r_c$, the minimal value of the activation energy is obtained by substituting $r = r_c$ in Eq. (13). The energy per unit length of the disconnection loop $q_D(r)$ is a slow-varying function of r that changes as $\ln(r)$. For simplicity, Faran and Shilo [47] assumed

that $q_D(r)$ can be taken as a constant. Thus, solving $\partial E_{DL}^{exsiting}/\partial r=0$ for r_c under these conditions results in:

$$r_c = \frac{q_D}{gd_{TB}} \tag{18}$$

The substitution of Eq. (18) in Eq. (13) provides an expression for the activation energy for the nucleation of a stable disconnection loop:

$$Q_{DL} = \frac{\pi \cdot q_{D}^{2}}{g \cdot d_{TB}} \left[\frac{3}{2} + \frac{\gamma_{TB}}{g \cdot d_{TB}} \right] \approx \frac{\pi \cdot \left(0.5 \mu b^{2} \right)^{2}}{g \cdot d_{TB}} \left[\frac{3}{2} + \frac{\gamma_{TB}}{g \cdot d_{TB}} \right]$$
(19)

In the second equality in Eq. (19) we introduced a rough approximation based on isotropic elasticity for the line energy of the disconnection $q_D \approx 0.5 \mu b^2$ (see page 169, Eqn. 6-51 in Ref. [72]).

The nucleation of a disconnection half-loop on the surface can be treated similarly, resulting in activation energy that is half the value expressed by Eq. (19).

5.3 Athermal heterogeneous nucleation of disconnections at the surface.

The topological structure of a coherently faceted type II boundary is inherently different from that of compound and type I, and contains a dense, ordered array of screw, misfit relieving disconnections (**Fig. 1** and related discussion in section 3). The disconnection array is preserved during motion of the interface. Thus, different nucleation mechanisms of disconnections are required to account for the motion of type II twins. In this section, we discuss a mechanism that enables athermal generation of disconnections on a type II TB. We evaluate and verify our analytical formulations by inserting material parameters for two representative material systems (10M Ni-Mn-Ga and Ni-Ti, see Table 2), in which type II twins play a significant role and the coherently faceted structure of the TB is well established.

We propose the following mechanism for the motion of a coherently faceted type II interface (Fig. 5). The twin boundary contains a regular disconnection array (as shown also in Fig. 1) in which the disconnection lines are parallel to the free surfaces. The parallelism assumption is valid for example when samples are cut with all faces along {100}. This is the case essentially for all published experimental results (e.g., Refs. [18,19,21–23,26,31,32,46,49,54,60]). Under an applied driving force, the slow-rate motion of this boundary (from top to bottom) involves two processes. One is the collective glide (from left to right in Fig. 5) of the disconnection array that advances the twin boundary perpendicular to its plane. Here we consider conditions under which the applied driving force enables disconnection glide over the Peierls barrier. As the disconnections reach the right surface they are emitted to the surface. Thus, a second process is required to occur simultaneously to maintain the topological structure and the motion of the TB: the nucleation of disconnections on the left surface. Next, we discuss conditions under which disconnections nucleate athermally.

Due to the disconnection glide, there is a region close to the left surface that becomes depleted of disconnections. The typical thickness of this region x_0 is much larger than the equilibrium spacing l_0 between disconnections in the array (as we show next). Therefore, this region is subjected to misfit elastic strains (as discussed in section 3) that are not accommodated by the disconnections array. The misfit strain builds up energy that grows with increasing x_0 . The tendency to reduce the elastic energy in this region results in a restoring force that pulls the array of disconnections back towards the left side. This force is not to be confused with the image force, which is caused due to the self-strain field of the disconnection. The tendency to reduce the elastic energy also encourages nucleation of disconnections on the left surface.

Recalling the low-energy configuration of the TB structure, presented in section 3, we assume that the equilibrium distance l_0 between disconnections is maintained during the motion of the array. This means that under an external driving force g_{TS} (that corresponds to the twinning stress) all disconnections move approximately the same distance x_0 , leaving a region with a width x_0 near the left surface that is depleted of disconnections **Fig. 5**(b). After a disconnection is nucleated on the left surface, **Fig. 5**(c), it moves to the right and joins the array of disconnections with equilibrium distance l_0 . The array of equally spaced disconnections forms a strain field that cancels out the misfit strain across the interface, except at the depleted region. Due to the misfit-

strain in the depleted region, the separation distance between the few furthermost disconnections at the left side of the array is larger than l_0 . As we show later, this does not alter the main results of our analysis, because $l_0 << x_0 << L$, where L is the width of the crystal.

In the following, we calculate the elastic energy due to the misfit strain. Further, we develop an expression for the equilibrium value of x_0 , and show that the misfit strain at the depleted region results in an additional energy term that promotes nucleation of disconnections at this surface. We develop an expression for the resulting activation energy and show that the term originated from the misfit strain may be dominant, thus promoting athermal nucleation. Then, we develop an expression for the equilibrium value of x_0 , and estimate x_0 for Ni-Ti and Ni-Mn-Ga. Further, we show that misfit strain at the depleted region results in an additional energy term that promotes nucleation of disconnections at this surface. We develop an expression for the resulting activation energy and show that the term originated from the misfit strain may be dominant, as is the case for Ni-Mn-Ga.

The strain field caused by the misfit shear in the region x_0 is equivalent to a strain field caused by an array of infinite number of equally-spaced coherency screw dislocations with an infinitesimal Burgers vector $db_{mis} = \varepsilon_0 dx$, such that the continuous integration of all Burgers vectors results in $\varepsilon_0 x_0$ [64,65]. The concept of coherency dislocations at an interface was introduced by Olson and Cohen (see, e.g., Refs. [77,78]), and was successfully applied by Speck *et al.* in modeling coherency strain at film/substrate interfaces of ferroelastic materials [79,80]. To maintain a zero stress near the left surface, we consider an equivalent array of image dislocations with a Burgers vector of the same size as the coherency dislocations but an opposite direction. The elastic energy associated with the coherency dislocations, per unit length perpendicular to the plane shown in Fig. 5, can be expressed as [79–81]:

$$E_{elastic}^{coh.disl.} = \frac{\mu (\varepsilon_0 x_0)^2}{4\pi} \ln \left(\frac{4L}{x_0} \right) \cong C \mu (\varepsilon_0 x_0)^2$$
(20)

where L is typically on the order of 1 mm and C is a constant on the order of unity.

The work associated with the motion of the TB under the driving force g_{TS} , per unit length perpendicular to the plane shown in Fig. 5, is given by

$$W_{TB}L \cong -g_{TS}Lx_0 \sin \theta \tag{21}.$$

Here, $\sin \theta x_0 \cdot L$ is the area (in the x-z plane) subjected to twinning reorientation due to the propagation of all disconnections in the array by a distance x_0 , where θ is the angle between the TB and the rational twinning plane (Fig. 5(b)).

To calculate the equilibrium value of x_0 , we minimize the overall energy (per unit length perpendicular to the viewing plane of **Fig. 5**) that includes the elastic energy in the depleted region, given by Eq. (20), and the work expressed in Eq. (21), i.e.,

$$\frac{\partial \left[C\mu \left(\varepsilon_0 x_0 \right)^2 - g_{TS} L x_0 \sin \theta \right]}{\partial x_0} = 0$$
 (22)

This results in:

$$x_0^{eq} = \frac{g_{TS} L \sin \theta}{2C \mu \varepsilon_0^2} \tag{23}$$

A substitution of material parameters listed in Table 2 and C=1, L=1mm in Eq. (23) provides $x_0^{eq} \cong 3 \ \mu m$ for Ni-Mn-Ga and $x_0^{eq} \cong 35 \ \mu m$ for Ni-Ti. These values satisfy the model assumption, $l_0 << x_0 << L$, as x_0 is larger than l_0 by few orders of magnitude and smaller than L by few orders of magnitude.

Next, we consider the lastly nucleated disconnection with a Burgers vector b, located at a distance $x_D < x_0$ from the left surface, as illustrated in Fig. 5(d). This disconnection is subjected to several interaction forces as it travels along x. The resultant force per unit length perpendicular to the plane shown in Fig. 5, is given by:

$$F = \frac{\mu b}{2\pi} \left[+ \int_{-x_0}^{0} \frac{\varepsilon_0 dx}{x_D - x} - \int_{0}^{x_0} \frac{\varepsilon_0 dx}{x_D - x} \right] - \frac{\mu b^2}{2\pi 2x_D} + F_{pK} - F_{peierls}$$
 (24).

The first two terms in Eq. (24) represent the sum of interaction forces between the left-handed screw disconnection b located at x_D and the array of coherency dislocations $db_{mis} = \varepsilon_0 dx$ located at $0 < x < x_0$. The image forces are accounted for by considering an equivalent array of image coherency dislocations $db_{mis} = -\varepsilon_0 dx$ at $-x_0 < x < 0$, as shown in Fig. 5(d). The term $\frac{\mu b^2}{2\pi 2x_D}$ in Eq. (24) is the image force of the disconnection b. F_{PK} is the Peach-Koehler force under the driving force g_{TS} , and $F_{Peierls}$ represents the resisting Peierls force acting on the moving disconnection by the lattice.

Our analysis considers conditions under which the driving force is sufficient to propagate the other disconnections along the TB. This means that the Peach-Koehler force is equal to, or greater than, the resisting Peierls force. Because we analyze a case where the resultant force on the lastly nucleated disconnection is always positive, we assume that $F_{PK} = F_{Peierls}$. Interaction forces due to the other disconnections in the array along the TB (not visible in **Fig. 5**(d)) are not included in Eq. (24) because, as stated earlier, at length scales larger than I_0 their strain field is canceled by the strain field of the misfit at the interface in their vicinity.

Solving the integrals and adding the disconnection's image force term in Eq. (24) results:

$$F = \frac{\mu b \varepsilon_0}{2\pi} \left(\ln \left[\left(\frac{x_0}{x_D} \right)^2 - 1 \right] - \frac{b}{2\varepsilon_0 x_D} \right)$$
 (25)

At the nucleation event $x_D \ll x_0$. In this region, the natural logarithmic term in Eq. (25) is a slowly varying positive function, while the last term in Eq. (25)) is negative and its magnitude increases rapidly as x_D decreases. The lower limit for x_D is taken as a single lattice spacing a, below which elasticity theory fails and the interaction forces described by Eqns. (24), (25) remain

nearly constant. Taking $x_D = a$, and inserting the values in Table 2, we obtain $\ln \left[\left(\frac{x_0}{x_D} \right)^2 - 1 \right] \cong 20$

for both Ni-Mn-Ga and Ni-Ti (the slow varying logarithmic term "alleviates" the one order of magnitude difference in x_0). In addition, $\frac{b}{2\varepsilon_0 a} \le 3.5$ for both materials, resulting:

$$F \cong (20 - 3.5) \frac{\mu b \varepsilon_0}{2\pi} = 8.25 \frac{\mu b \varepsilon_0}{\pi}$$
 (26),

This indicates that in the range relevant for the nucleation event, $x_D \ll x_0$ the force F is always positive and pushes the disconnection towards the right side. Consequently, the self-energy E_D^{self} of the disconnection that nucleates at the surface (i.e., at $x_D \cong a$) is negative and is given by:

$$E_D^{self} = Y \int_0^{x_D} -F dx_D = -Y a \cdot 8.25 \frac{\mu b \varepsilon_0}{\pi}$$
 (27)

where Y is the disconnection length in the direction perpendicular to the plane shown in Fig. 5. Next, we use this result to evaluate the activation energy for the heterogenous nucleation process. In section 5.2 (Eq. (13)) we obtained a general expression for the activation energy for nucleation of a disconnection loop, Q_{DL} . Similarly, the activation energy for nucleation of a linear disconnection, Q_D , is given by:

$$Q_D = U_{TB}^{bar} \cdot A + E_D^{self} \tag{28}.$$

Here $A \cong Ya$ is the area of the TB that has been reoriented by the formation of the disconnection at $x_D \cong a$, and U_{TB}^{bar} is the energy barrier imposed by the lattice potential, as expressed in Eq. (14). Substituting Eq. (14) (for U_{TB}^{bar}) and Eq. (27) (for E_D^{self}) into Eq. (28). Provides

$$Q_D = Ya \cdot d_{TB} \left(\frac{g_0}{\pi} - \frac{g}{2} - 8.25 \frac{\mu \varepsilon_0 b}{\pi d_{TB}} \right)$$
(29)

Recalling that b/h = s, and that the periodicity of the lattice potential approximately equals to the disconnection step height (i.e., $d_{TB} \approx h$), we obtain the following expression for the activation energy for the nucleation of a disconnection at the surface.

$$Q_D = Ya \cdot h \left(\frac{g_0}{\pi} - \frac{g}{2} - 8.25 \frac{\mu \varepsilon_0 s}{\pi} \right) \tag{30}$$

In cases where $8.25\mu\epsilon_0 s > g_0$, Q_D in Eq. (30) is negative for any value of the applied driving force g, indicating that this nucleation process can occur athermally. This condition is determined only by material properties and can be evaluated based on the values listed in Table 2. For 10M Ni-Mn-Ga $8.25\mu\epsilon_0 s \cong 20 \cdot 10^6$ J/m³, and is larger than $g_0 \cong 85 \cdot 10^3$ J/m³ by several orders of magnitude (see Ref. [47]). For Ni-Ti, $8.25\mu\epsilon_0 s \cong 500 \cdot 10^6$ J/m³, indicating that this nucleation process can occur athermally if $\gamma_{TB} < 30\,\mathrm{mJ/m^2}$ (recall that $g_0 = \pi\gamma_{TB}/d_{TB}$). Such a value of γ_{TB} is comparable to atomistic calculations reported by Sehitoglu *et al.* [70].

We now re-evaluate the model assumption that the equilibrium distance l_0 between disconnections is maintained during the motion of the array, such that all disconnections move approximately the same distance x_0 , leaving a region with a thickness x_0 depleted of disconnections. To hold this assumption, the lastly nucleated disconnection has to be subjected to a positive force (Eq. (25)), until it meets the other disconnections in the array. The force is indeed positive for all values of x_D smaller than $\frac{\sqrt{2}}{2}x_0$. For larger values of x_D , Eq. (25) predicts that the net force on the disconnection becomes negative. However, when the disconnection reaches a value of x_D that is on the order of x_0 , it can be regarded as being part of the disconnection array that composes the TB. This is in accordance with our previous comment, stating that the leftmost disconnections in the array are spread apart a distance that is larger than the equilibrium value l_0 .

This relaxation has a minor effect on the elastic energy estimated by Eq. (20) and hence on the estimated value of x_0^{eq} provided by Eq. (23). Further, the exact value of x_0 has a minor effect on the evaluation of the force F (using Eq. (25)) in the range, $x_D << x_0$, relevant for the nucleation event. We disregard these effects in the current treatment.

Finally, because the model relies on nucleation at the surface, we evaluate the case of sub-mm size samples, e.g., micropillars, where surface to volume ratio is much larger compared to ordinary mm-size crystals. In particular, the relation $l_0 << x_0 << L$ (see Eq. (23)) remains valid even for values of L that are on the order of few tens of microns (typical to micropillars). Thus, the increase in twinning stress observed in some 10M Ni-Mn-Ga micropillars can be associated with the presence of defects that hinder TB motion, and result from the unique fabrication process of the pillar [82,83]. In case the crystal size is further decreased, such that our model assumptions are no longer valid, we expect the twinning stress to increase, because the proposed mechanism of athermal disconnection nucleation may not be relevant in such scales.

Table 2: Typical material parameters for type II twins in 10M Ni-Mn-Ga and Ni-Ti.

	10M Ni-Mn-Ga	NiTi
μ (GPa) *	[11,84]	□ [85,86]
\mathcal{E}_0	0.0092 [42]	0.049 [44]
S	0.127 [42]	0.28 [44]
θ	4.12° [42]	10.11° [44]
l_0 (nm)	☐ [42]	□ [44]
a (nm)	☐ [18]	□ [87]
b (nm)	0.023 [42]	0.071 [44]
g_{TS} (J/m ³)	$1.3 \cdot 10^4$ [88]	☐ [70] **
$x_{_{0}}^{eq}$ (µm)	[Eq. (23)]	[Eq. (23)]

^{*} Value of shear stiffness μ in the isotropic elasticity formulation is related to the elastic constant C'.

Commented [PM3]: Critical Stresses for Twinning, Slip, and Transformation in Ti-Based Shape Memory Alloys

•<u>A. Ojha</u> &

•<u>H. Sehitoglu</u>

Shape Memory and

Superelasticity volume 2, pages180–195 (2016)

Commented [PM4]: Ojha and Sehitoglu 2016 give a value of 25 MPa.

Commented [e5R4]: This paper deals with Ni-Nb-Ta alloys. I could not find a value for the TS of type II in NiTi....

^{**} Value is estimated based on a twining stress of $\sigma_{TS} \cong 20$ MPa [REF?].

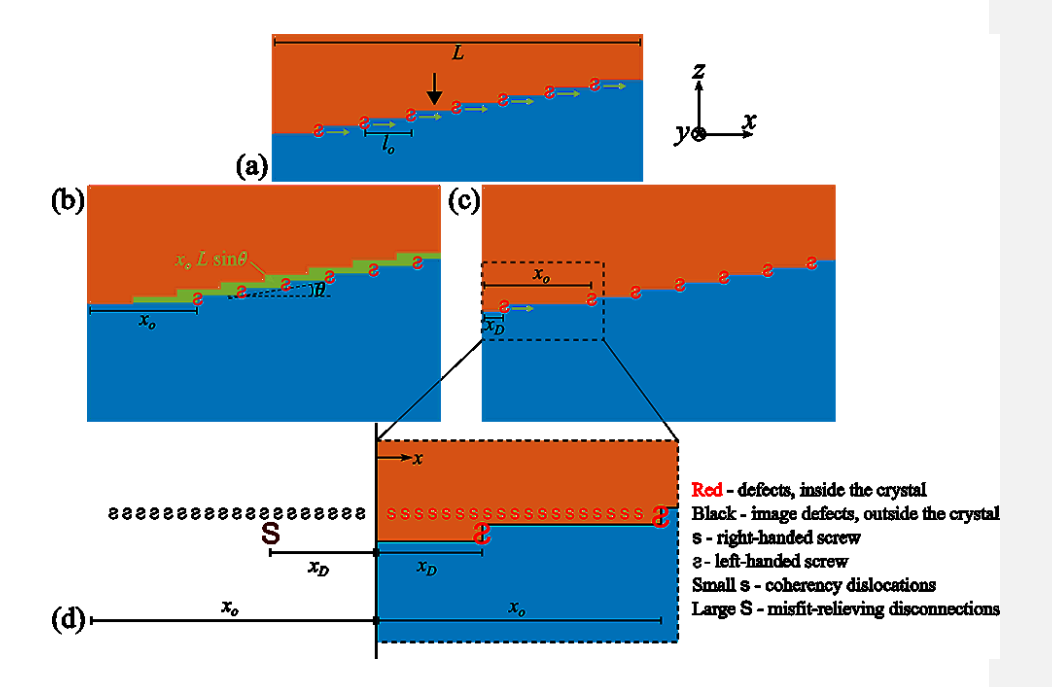


Fig. 5 Schematic description of the equilibrium coherently faceted type II interface (inset (a)), that contains an array of left-handed screw disconnections, which are marked with an inverted 'S'. L marks the width of the crystal. Under an applied driving force, the disconnections move to the right (green arrows), transforming material from the top variant to the bottom (the green area in inset (b)), leading to the advancement of the TB downwards (direction marked by the vertical black arrow). The collective motion of the disconnection array creates a "depleted" region of length x_0 close to the left surface (inset (b)). To maintain the coherently faceted structure, disconnections nucleate at the left surface and propagate to the right (inset (c)). The position x_D marks the location of a newly nucleated disconnection relative to the left surface. (d) A schematic illustration of the depleted region x_0 close to the surface with a representation of the disconnections (large S with Burgers vector b) and coherency dislocations (small S with burgers vector db_{mis}). Image defects maintain zero stresses on the free surface (the vertical black line).

6. Kinetic relations for TB motion, rate-limiting processes and twinning stress

In this section, we formulate relations between the different activation energies developed in section 5 and the measured quantities that represent the mobility of the different types of TB's, and in particular the twinning stress. This analysis relies on the kinetic relation, which provide an analytical expression for the velocity of a TB as a function of the driving force, and is dictated by the rate limiting process of the overall TB motion. We focus on TB motion in the low driving force range, and discuss separately the situations of compound and type I twins (section 6.1, which is based on the analysis in sections 5.1 and 5.2) and type II twins (section 6.3, which is based on section 5.3).

6.1 Kinetic relations

To study the kinetic relations, the twin boundary velocity v_{TB} has to be measured under different values of the driving force. This is in contrast to measuring the twinning stress, which occurs at a constant value, g_{TS} , of the driving force. Kinetic measurements were performed mainly on the 10M Ni-Mn-Ga material system, using μs - scale pulsed magnetic field experiments, as reported by Faran and Shilo [46,47] and by Saren et al [48,89]. Recently, fast TB motion in 10M Ni-Mn-Ga was also studied by short ms-scale force pulses [90–92].

Faran and Shilo [46,47] measured the kinetic relations in a systematic manner by applying magnetic pulses with controlled values of the driving force and tracking the motion of a discrete twin boundary. They captured the kinetic relations for twin boundary motion in 10M Ni-Mn-Ga over a wide range for driving force and TB velocity. For both type I and II twins, they found a clear transition between two types of kinetic relations, as is explained herein.

For the thermally activated regime of TB motion (i.e. at low driving force), an exponential type kinetic relation for the twin boundary velocity v_{TB} can be assigned:

$$v_{TB}(g) = v_0 \exp\left(\frac{-Q(g)}{nkT}\right)$$
(31)

In Eq. (31), v_0 is a temperature-independent pre-exponent term, Q(g) is the activation energy of the rate limiting process, which is a function of the driving force g, and n is a parameter that represents the dimension of the problem (following the analysis of Avrami in Refs. [93,94]). For example, for the nucleation of a two-dimensional disconnection loop, n=3, while for nucleation of a linear kink n=2.

In slow rate experiments, where a constant deformation rate is applied, the average velocity of an individual TB $v_{TB}^{(TS)}$ (i.e., the velcoity associated with the measured twinning stress property) is determined by the number of moving twin boundaries in the sample and the applied strain-rate (e.g., Ref. [88]). Therefore, the set value of the velocity $v_{TB}^{(TS)}$ in Eq. (31) determines the twinning stress σ_{TS} or the related value of the driving force, $g_{TS} = \sigma_{TS} \cdot s/2$ (Eq. (3)), at which TB motion occurs, via:

$$Q(g_{TS}) = nkT \ln \left(\frac{v_0}{v_{TB}^{(TS)}} \right)$$
(32)

As we show in the next sections, for type I twins, the activation energy corresponds to Q_{DL} (see section 6.2) while for type II it corresponds to Q_{KP} (see section 6.3).

In the study by Faran and Shilo on 10M Ni-Mn-Ga [46,47], it was found that above some transition value of the driving force g_T , the kinetic relation had the form

$$v_{TB} \propto \sqrt{g^2 - {g_T}^2} \tag{33},$$

indicating a process that is resisted by viscous forces. Similar types of viscous-controlled kinetic relations were suggested for data measured in other material systems such as Cu-Al-Ni [95] and gadolinium molybdate [96].

Faran and Shilo [46,47] suggested that the transition at g_T is attributed to overcoming the lattice barrier for the motion of the TB as a flat plane, γ_{TB} (as shown in Table 1), resulting in athermal

motion of the TB. According to that interpretation, the transition driving force is directly related to the lattice barrier via

$$g_T = g_0 = \frac{\pi \gamma_{TB}}{d_{TR}} \tag{34}$$

For type I twins in 10M Ni-Mn-Ga, the transition driving force was $g_0 = 105$ kJ/m³ [47], relating to a stress of approximately 1.75 MPa, i.e., about twice the twinning stress for this type of twin [23]. For type II twins, the transition driving force was $g_0 = 85$ kJ/m³ [47] related to a stress of approximately 1.4 MPa, i.e., ten times the twinning stress for this twin type [23].

6.2 Motion of compound and type I twins in the low driving force range

The rate limiting process for the motion of compound and type I twins in the slow velocity range is either the nucleation of kink-pairs or nucleation of disconnection loops. The two processes are characterized by their activation energies Q_{KP} and Q_{DL} , given by Eq. (12) in section 5.1 and Eq. (19) in section 5.2, respectively.

In order to evaluate which energy dominates, we consider the ratio between the two activation energies at a driving force equivalent to the twinning stress, i.e., at $g_{TS} = \frac{\sigma_{TS} \cdot s}{2}$. Specifically, we use an under-estimation of Q_{DL} (by neglecting the positive γ_{TB} term in Eq. (19)) and consider only the dominant term $2e_f$ in the expression for Q_{KP} (Eq. (12)). This results in:

$$Q_{DL} / Q_{KP} \ge \frac{3}{2} \frac{\pi \cdot \left(0.5 \mu b^2\right)^2}{g_{TS} \cdot d_{TB}} \left(\frac{1}{2e_f}\right)$$
(35)

Using an isotropic approximation for the formation energy of a kink $2e_f \approx \mu b^2 d_D$ (see section 5.1), and substituting $g_{TS} = 0.5\sigma_{TS} \cdot s$, $b = h \cdot s$ and $h \approx d_D \approx d_{TB}$, we obtain

$$Q_{DL} / Q_{KP} \ge s \frac{\mu}{\sigma_{TS}} \tag{36}$$

The ratio μ/σ_{TS} is typically several orders of magnitude larger than unity for all material systems and the value of s is typically on the order of 0.1 (see, e.g., values in Table 2, Table 3). Thus, we can conclude that for the lower driving force range, the activation energy Q_{DL} is much larger than Q_{KP} .

The above discussion implies that in the thermally activated regimes, the nucleation of disconnection loops is the rate-limiting step in the overall motion of the TB for compound and type I twins. Even if the driving force does not allow overcoming the Peierls barrier for disconnection glide, i.e., $g < (\pi \cdot \Gamma_D / d_D \cdot h)$, the thermally activated disconnection glide is still a faster process than the thermally activated disconnection nucleation, because $Q_{DL} >> Q_{KP}$. Thus, inserting Q_{DL} (Eq. (19) as the activation energy in the kinetic relation for compound and type I twins (Eq. (32)) results in:

$$Q_{DL}(g_{TS}) \approx \frac{\pi \cdot \mu^2 s^3 \cdot d_{TB}^3}{2\sigma_{TS}} \left[\frac{3}{2} + \frac{2\gamma_{TB}}{\sigma_{TS} \cdot s \cdot d_{TB}} \right] = 3kT \ln \left(\frac{v_0}{v_{TB}^{(TS)}} \right)$$
(37)

Here we used the relations $g_{TS} = 0.5 \cdot \sigma_{TS} \cdot s$ and $b = h \cdot s \approx d_{TB} \cdot s$.

Typically, the value of $v_{TB}^{(TS)}$ is smaller than v_0 by many orders of magnitude. Therefore, a change of $v_{TB}^{(TS)}$ by an order of magnitude results in a minor change of $\ln\left(v_0/v_{TB}^{(TS)}\right)$, which is often undetectable due to the inherent stress fluctuations and insufficient repeatability that are common in such experiments. For example, based on intermediate-rate experiments performed on 10M Ni-Mn-Ga single crystals, Faran and Shilo extracted the value $v_0 = 6.6 \ m/s$ for type I boundary [47]. A typical twin boundary velocity in a slow rate experiment is $v_{TB}^{(TS)} = 10^{-5} \ m/s$ [97]. For these values, a change of $v_{TB}^{(TS)}$ by an order of magnitude results in a change of Q_{DL} by 17%, which is comparable to the variations of the approximately plateau stress during the experiment. Thus, the

estimation of the term $\ln\left(\frac{v_0}{v_{TB}^{(TS)}}\right) \approx 13.4$ can be assumed to be valid in most SMA. Inserting this approximation in Eq. (37) results in:

$$\frac{\pi \cdot \mu^2 s^3 \cdot d_{TB}^3}{2\sigma_{TS}} \left[\frac{3}{2} + \frac{2\gamma_{TB}}{\sigma_{TS} \cdot s \cdot d_{TB}} \right] = 40kT$$
 (38)

Eq. (38) allows estimating the magnitude of the twinning stress σ_{TS} , and its temperature dependence, provided that the material properties $\mu, s, d_{TB}, \gamma_{TB}$ are known. We note that a measured value for γ_{TB} is available only for 10M Ni-Mn-Ga.

6.3 Motion of type II twins in the low driving force range

In section 5.3 we presented a mechanism of motion for type II TB, which results from the topological structure of this twin type. Our analyses identified that heterogeneous nucleation of disconnections at the surface is essential for TB motion, and an expression for the activation energy for such a nucleation process was formulated in Eq. (30). Further, we showed that for certain materials, such as Ni-Mn-Ga, the expression for the activation energy obtains negative values for any value of the applied driving force, implying that nucleation of disconnections occurs athermally. In these materials the twinning stress of type II TB is related solely to the glide of disconnections. This is in contrast to the case of compound and type I TBs, for which disconnection nucleation is the rate limiting step that determines the twinning stress (section 6.1).

Similar to the motion of ordinary dislocations, disconnection glide proceeds through the nucleation and expansion of kink-pairs, where nucleation is typically the rate limiting step. Consequently, for a type II TB, the thermally activated kinetic relation (Eq. (31)) is dictated by the activation energy for the nucleation of kink-pairs (Q_{KP} in Eq. (12)). The combination of these two expressions, and by substituting $g = g_{TS}$, results in:

Commented [Bk6]: Maybe add $Q_{DL}(g_{TS}) = ...$

Commented [PM7]: Is this true for ALL materials including structural materials or only for shape memory alloys? Steels seems to fall outside the prediction in Fig. 6.

$$Q_{KP}(g_{TS}) \approx \left(\Gamma_D - \frac{g_{TS} \cdot h \cdot d_D}{2}\right) y_c + \left(2e_f - \frac{e_{\text{int}}}{y_c}\right) = 2kT \ln\left(\frac{v_0}{v_{TB}^{(TS)}}\right)$$
(39)

An estimation for the amplitude of the disconnection's Peierls barrier Γ_D can be obtained from the condition $g > (\pi \Gamma_D)/(d_D h)$ that defines the driving force range of athermal disconnection glide, i.e., the driving force required to overcome the Peierls barrier Γ_D at $T=0\,K$. Thus, we can write

$$\Gamma_D \le g_{TS} (T = 0K) d_D h / \pi \tag{40}$$

By inserting the expression for Γ_D (Eq. (40)) and y_c (Eq. (11) in section 5.1) into Eq. (39) and rearranging, we obtain:

$$\left(\frac{g_{TS}\left(T=0\,K\right)}{\pi g_{TS}\left(T\right)} - \frac{3}{2}\right) \sqrt{g_{TS}\left(T\right) \cdot e_{\text{int}} \cdot h \cdot d_{D}} + 2e_{f} = 2kT \ln\left(\frac{v_{0}}{v_{TB}^{(TS)}}\right)$$

$$(41)$$

Here, $g_{TS}\left(T\right)$ represents the driving force associated with the twinning stress at a temperature $T>0\,K$. Eq. (41) may have various solutions for $g_{TS}\left(T\right)$, depending on the ratio between $2kT\ln\left(\frac{v_0}{v_{TB}^{(TS)}}\right)$ and $2e_f$. In section 7.3 we discuss experimental data measured for 10M Ni-Mn-Ga in light of this analysis.

7. Comparison of model predictions to experimental results

The identification of the different nucleation processes required for TB motion and their associated activation energies (section 5), as well as the identification of the rate limiting processes for different twin types (section 6) allows us to quantitatively evaluate our predictions and compare them to experimental results for TB motion. Because the analysis presented in this paper considers

only the lattice barrier as the source for the twinning stress, comparison to experiments is meaningful primarily for data measured on high quality single crystals, where the effects of other barriers is negligible. For example, grown Ni-Ti single crystals typically include nanoscale Titanium carbides and Ni-rich precipitates, which strongly influence the mobility of the TB's (see, e.g., [17]). Thus, twinning stress values measured in such cases are expected to be higher than our predictions.

In the following sections we discuss results from slow-rate deformation experiments with strain rates below about 10⁻² s⁻¹, which have been studied extensively for various shape memory alloys. These low strain rates correspond to the small driving force regime. The primary measured parameter that characterizes TB motion within this regime of motion is the twinning stress (defined in section 2). Available experimental values for the twinning stress raise several questions, which we address in the following sections by employing the equations developed in section 6.

In section 7.1 we explain why the twinning stress at room temperature of type II twins is much smaller than that of type I twins in the same material. In section 7.2 we employ Eq. (38) to predict the values of the twinning stress of compound and type I twins in different materials, and compare our predictions to experimental data. In addition, we reason the measured temperature dependence of the twining stress (available mainly for 10M Ni-Mn-Ga). In section 7.3, we reason the unique temperature insensitivity of type II twinning stress, as demonstrated by very low values measured for 10M Ni-Mn-Ga down to near zero temperatures.

7.1 Differences in twinning stress between twin types.

Available experimental data reveals a large difference between the measured twinning stress of conjugate type I and type II twins in the same alloy, the latter being significantly smaller. This is the case, for example, in 10M Ni-Mn-Ga, where differences as high as one order of magnitude are commonly reported between the twinning stress of conjugate type I and type II twins [18]. Similar relations were reported for conjugate type I and type II twins in Cu-Al-Ni [19,31] and in Ni-Ti [17,98,99].

The term conjugate twins implies that the classical twinning elements of both twins, i.e., twinning planes K_1, K_2 , twinning directions η_1, η_2 , and twinning shear s, obey $K_1^{II} = K_2^{I}, K_2^{II} = K_1^{I}, \eta_1^{II} = \eta_2^{I}, \eta_2^{II} = \eta_1^{I}$ and $s^{I} = s^{II}$. Thus, the twinning shears of both types are

identical. Moreover, variations in lattice parameters that directly affect the magnitude of the twinning shear, as well as the value of the shear stiffness are identical in the two twin types. The TM shows that the magnitudes of the Burgers vector and the step height of a disconnection in "conjugate" type I and type II twins, are nearly equal (e.g., the calculations performed for 10M Ni-Mn-Ga in [42]). Thus, by discussing differences in the twinning stress between "conjugate" twins in the same alloy we separate the effect of the topological structure of the TB that dictates the rate limiting mechanism of motion, from the impact of material properties (e.g., shear stiffness twinning shear and lattice spacing), which are discussed in section **Error! Reference source not found.**

The different topological structures of type I and type II twins (section 3) lead to different rate limiting mechanisms during TB motion (sections 5 and 6). On the one hand, the motion of type I TB is determined by the rate of homogenous nucleation of disconnection loops on the low index boundary plane, with an activation energy Q_{DL} . On the other hand, the motion of a coherently faceted type II TB is determined by the rate at which disconnections glide on the same low index planes. For type II TBs, disconnection glide is dictated by the nucleation rate of kink-pairs, with an activation energy Q_{KP} . As we showed in section 6.2, $Q_{DL} >> Q_{KP}$ for a given material system. Thus, the activiation energy for type II TB motion (which is Q_{KP}) is much smaller than the activation energy for type I TB motion (which is Q_{DL}). This implies that the twinning stress of a type II twins is much lower than that of type I and the temperature dependence is much weaker, in agreement with experiemmntal observations.

7.2 Twinning stress of compound and type I twins

The twinning stress of compound and type I twins in a given material can be approximated based on Eq. (38), provided that the properties μ , s, d_{TB} , γ_{TB} are known. We first analyze the situation in which the term containing γ_{TB} in Eq. (38) is much smaller than 3/2, and can thus be neglected (which is the case for 10M Ni-Mn-Ga). This results in a simplified expression for the twinning stress:

$$\sigma_{TS} \cong \frac{3\pi}{160kT} d_{TB}^{3} \mu^{2} s^{3} = \beta \mu^{2} s^{3}$$
(42)

The value of the lattice spacing for twinning d_{TB} is similar for different SMA, and can be taken as $d_{TB}=0.2\,\mathrm{nm}$ for all materials. Under these conditions, Eq. (42) predicts a linear relation between the twinning stress σ_{TS} and the product $\mu^2 s^3$, with a proportionality factor $\beta=\frac{3\pi}{160kT}d_{TB}^3$. This relation, for the twinning stress at the room temperature, is plotted as the solid black line in **Fig. 6** using logarithm scaling of the variables. In this representation, the straight-line has a slope of 1 and it intercepts the vertical axis at β .

Experimental data for different materials is also plotted in **Fig. 6**, using the same logarithm scaling. The values of μ and s used for plotting the data for each twinning system and material were reported in the literature and are given in Table 3. The dashed line in **Fig. 6** presents the relation express in Eq. (42) with a proportionality factor $\beta' = 0.64\beta$ that best fits the experimental data. The relatively small difference between β and β' can be attributed to the estimations we took in Eq. (37), e.g., the value of 13.4 assigned to the term $\ln\left(v_0/v_{TB}^{(TS)}\right)$, or the factor 0.5 in the isotropic approximation $q_D \approx 0.5 \mu b^2$.

The good fit to a linear dependence of the measured twinning stress with the product $\mu^2 s^3$ (dashed line in **Fig. 6**, R-squared larger than 0.99) strengthens the validity of our analysis. In addition, it implies that our assumption $\frac{2\gamma_{TB}}{\sigma_{TS}\cdot s\cdot d_{TB}} \leq 3/2$ is valid in most materials. Recalling that $g_{TS} = \sigma_{TS}\cdot s/2$ (Eq. (3)) and $g_0 = \pi\gamma_{TB}/d_{TB}$ (Eq. (34)), the relation $2\gamma_{TB}/\sigma_{TS}\cdot s\cdot d_{TB} \leq 3/2$ implies that $g_0 \leq 5g_{TS}$. This means that for most materials a transition from thermally activated

Commented [PM8]: I put this into a footnote because it seems to disrupt the flow of the paper otherwise. Also, the footnote text really is about materials that do NOT fall into the scope of this paper. Nonetheless, I think the addition is valuable in the broader context of twinning. I suggest the following reference to be included in the footnote:

```
Twinning-induced plasticity (TWIP) steels

1.By

De Cooman, BC (De Cooman, Bruno C.) 1Estrin, Y (Estrin, Yuri) 2, 3Kim, SK (Kim, Sung Kyu) 4

View Web of Science ResearcherID and ORCID (provided by Clarivate)
ACTA MATERIALIA

2.Volume

142

3.Page
283-362

4.DOI
```

10.1016/j.actamat.2017.06.046

¹ Equation (42) does not apply to materials for which the nucleation of disconnection loops is not the rate limiting mechanism. For example, for face-centered cubic (austenitic, twin-induced plasticity, TWIP) steel $\mu^2 s^3$ is in the order of 10^4 GPa² and Equation (42) predicts a twinning stress about three orders of magnitude higher than actual values. In these materials, substantial deformation by slip precedes the onset of twinning. Twin nucleation results from dislocation reactions at sites of high dislocation density and strong stress concentrations. The stress concentrations result from dislocation pileups of dozens or hundreds of dislocations. Accordingly,

motion to fast athermal TB motion is expected to occur at stress values equal or smaller than 5 times the twinning stress. Measured values of g_0 and g_{TS} in 10M Ni-Mn-Ga comply with this condition (see discussion in section 6.1).

In a rough approximation, at which the temperature effect on the shear modulus and twinning stress is ignored, Eq. (42) predicts that the temperature variation of twinning stress of compound and type I twins follows an inverse 1/T relation. Data reported in Ref. [32] for a type I twin in 10M Ni-Mn-Ga revealed a linear increase in the twinning stress as the temperature decreases (**Fig. 7**). Data measured over a wider range of at least 100 degrees in 10M Ni-Mn-Ga [30,34,100] showed a variation that can be interpreted as $\sigma_{TS} \propto 1/T$ (**Fig. 7**). A similar dependence was recently reported for compound twins in Ni-Mn-Ga-Co-Cu [101] and type I twins in 4M Ni-Mn-Sn alloy [21]. These observations rely on measurements taken over a relatively narrow temperature range of about 40 degrees.

The calculated temperature dependence according to Eq. (42), with μ and s takes as their room temperature values, for type I twin in 10M Ni-Mn-Ga is plotted in Fig. 7 (blue dashed line), showing a weaker dependence on temperature compared to the measured data. We can reason this difference by considering the effects of the temperature on product $\mu^2 s^3$. Both the shear stiffness (again we refer to μ as the elastic constant C') [102–104], and the twinning strain [105] increase as the temperature is decreased, and thus amplify the 1/T dependence in Eq. (42). In addition, for materials in which $2\gamma_{TB}/\sigma_{TS}\cdot s\cdot d_{TB}$ is comparable to 3/2, the dependence of γ_{TB} on the temperature (as was reported in Ref. [106]) also contributes to the temperature effect on the twinning stress.

Table 3: Material properties and measured data used for plotting (in Fig. 6) the room temperature twinning stress of type I and compound twins in several materials.

dislocation reactions resulting in partial (twinning) dislocations and disconnections occur at stresses several orders of magnitude below the stress predicted by Equation (42). [REF]

	10M	NM	Cu-Al-Ni	Cu-Al-	BaTiO ₃	NiTi
	Ni-Mn-	Ni-Mn-Ga		Ni		
	Ga					
Twin	Type I	Compound	Compound	Type I	Compound	compound
type						
μ	2	2	9.14	9.14	50	5 [85,86]
(GPa)	[11,84]	[11,84]	[31]	[31]	[107]	
S	0.127	0.36	0.074	0.26	0.0109	0.2385
	[42]	[108]	[31,109]	[31]	[6]	[44]
$\sigma_{\scriptscriptstyle TS}$	0.8	11	2	>100	0.25	25
(MPa)	[18]	[110,111]	[19]	[31]	[6]	[17]
(exp.)						

Commented [CU9]: I tried twinning in austenitic steel (compound twinning) and found that it fall far below the trend. I assume this is because the formation of disconnection loops is not the rate limiting process. Instead, twinning disconnections form from dislocation reactions which occurs at lower stress than the formation of disconnection loops. While this observation is not directly related to shape memory alloys, it does fit into the overall picture. Do we want to add a short paragraph along these lines?

Yes Peter – please insert this discussion, either here or in the summary

The legend says Eq. (40) for the solid line but it should be Eq. (42). Corrected

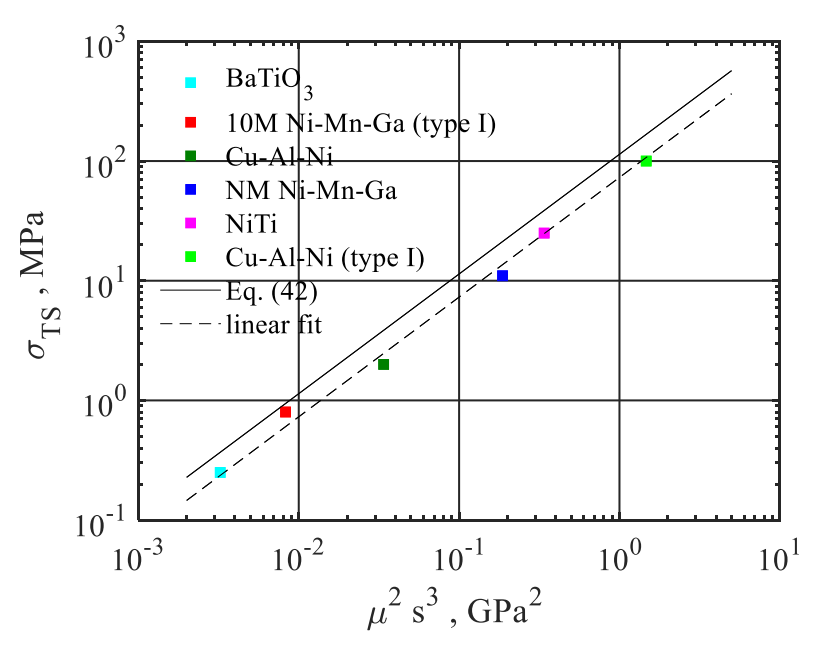


Fig. 6 Twinning stress at room temperature versus the product $\mu^2 s^3$ for compound and type I twins in several SMA systems, presented on logarithm scales. Data for different alloys were taken from Table 3. The dashed grey line is a linear fit to the experimental data, exhibiting $R^2 > 0.99$. The solid black line represents the calculated relation given by Eq. (42).

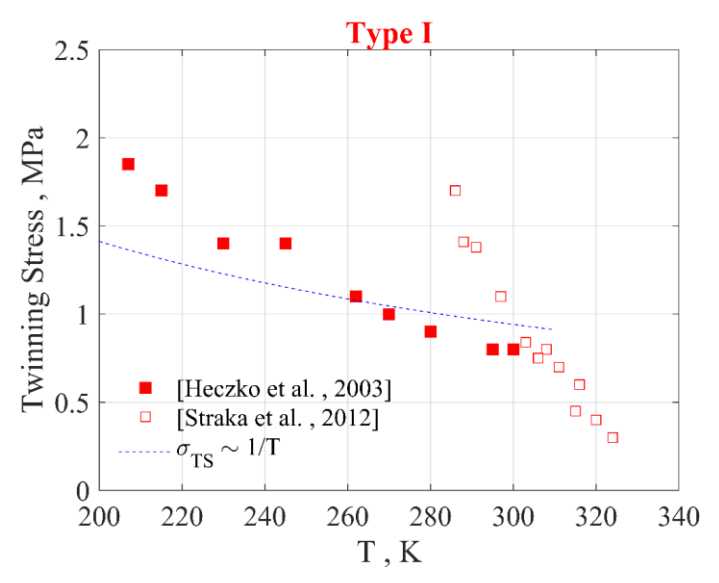


Fig. 7 Temperature variation of the twinning stress of type I twin in 10M Ni-Mn-Ga. Experimental data is taken from Refs. [32,34]. The dashed blue line represents the 1/T dependence obtained from Eq. (42), using the room temperature values of μ and s listed in Table 3.

7.3 Twinning stress of type II twins

Information on the twinning stress of type II TBs is available mainly for Cu-Al-Ni and 10M Ni-Mn-Ga, the latter being extensive and measured on high quality single crystals over a large temperature range. In the following, we discuss data obtained for 10M Ni-Mn-Ga, which reveals two interesting behaviors: (1) an extremely small twinning stress of approximately 0.25 MPa at 1.7 K and (2) a modest temperature sensitivity of the twinning stress over a range of 300 K (see Fig. 8).

In section 6.3, we obtained an expression for the temperature dependence of the driving force associated with the twinning stress (Eq. (41)). We assumed that the type II TB motion follows an exponential type kinetic relation (Eq. (31)), which is dictated by the activation energy for the nucleation of kink-pairs Q_{KP} (Eq. (12)). This approach is valid in case the activation energy Q_{KP} is smaller than the thermal energy, and resulted in:

$$\left(\frac{g_{TS}\left(T=0\,K\right)}{\pi g_{TS}\left(T\right)} - \frac{3}{2}\right) \sqrt{g_{TS}\left(T\right) \cdot e_{\text{int}} \cdot h \cdot d_{D}} + 2e_{f} = 2kT \ln\left(\frac{v_{0}}{v_{TB}^{(TS)}}\right)$$

$$(43)$$

The data presented in **Fig. 8** indicates that for 10M Ni-Mn-Ga, $\frac{g_{TS}\left(T=0K\right)}{\pi g_{TS}\left(T\right)} < \frac{3}{2}$ over the temperature range $0 < T \le 300K$. Thus, if Eq. (43) is valid then $2e_f$ should be larger than $2kT \ln\left(\frac{V_0}{V_{TB}^{(TS)}}\right)$, for any temperature up to $T \cong 300K$. Recalling that $2e_f \cong \mu b^2 d_D \cong \mu s^2 d_D^3$ (the first equality follows page 244, Eqn. 8-47 in Ref. [72], and the second equality is obtained by taking $b=h\cdot s\approx d_D\cdot s$) and plugging typical material parameters for type II twins in 10M Ni-Mn-Ga (Table 2), yields $2e_f \cong 2.5 \times 10^{-22}$ J. Thus, already for temperatures as low as T=10K, the term $2e_f$ (which determines the magnitude of the activation energy) is smaller than the thermal energy term, $2kT_{(T=10K)} \ln\left(\frac{V_0}{V_{TB}^{(TS)}}\right) \approx 30kT_{(T=10K)} \cong 4 \times 10^{-21} \, \mathrm{J}$. This implies that for 10M Ni-Mn-Ga, the description of the nucleation-controlled kinetics of type II TB motion by an exponential relation (Eq. (31), which leads to the formulation of Eq. (43)) is not valid. Moreover, because the activation energy for nucleation of kink pairs is comparable to the thermal energy even at very low temperatures, thermally activated disconnection glide, which is weakly dependent on temperature and proceeds at very low stress, is possible down to very low temperatures. This agrees with the experimental data in **Fig. 8**.

In other materials, the magnitude of $2e_f$ is larger than the value for 10M Ni-Mn-Ga (e.g., in Cu-Al-Ni it is \Box times larger). However, there is no experimental data on the value of $\sigma_{TS}(T=0K)$ in other materials, and it may be much larger than the value at room temperature, such that $\frac{g_{TS}(T=0K)}{\pi g_{TS}(T)} > \frac{3}{2}$, and $2e_f >> kT$ over a wide temperature range. Under these conditions the analysis leading to Eq. (43) is valid. In such cases, the twinning stress of type II TB is also expected to be larger than the extremely low values measured for 10M Ni-Mn-Ga.

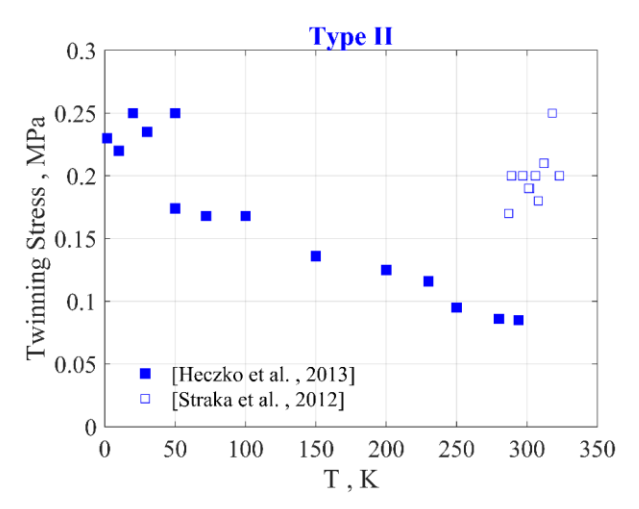


Fig. 8 Temperature variation of the twinning stress of type II twins in 10M Ni-Mn-Ga. Experimental data is taken from Refs. [30,32]. The temperature dependence is substantially weaker than that of the conjugate type I twins (**Fig. 7**).

8. Summary

This paper combines the TM descriptions for the equilibrium structures of TB in SMA with an analysis of energy barriers and mechanisms of motion. This unified approach provides a general analysis of TB motion and explains experimental findings on TB motion in different SMA systems, in particular in the slow rate regime of TB motion. We identify the topological, structural aspects that control the rate limiting mechanisms of motion of different twin types, and deduce quantitative predictions for the magnitude and temperature dependency of the twinning stress of different twin types.

The slow rate motion of TB is controlled by different rate-limiting processes, which are dictated by the equilibrium topological structure of the TB interface. For type II twins, we discuss the case of a coherently faceted interface, which contains an ordered array of equally spaced twinning disconnections. We show that for this low-energy relaxed structure, the nucleation of new disconnections at the crystal's surface, which is essential for maintaining the lateral

propagation of the TB, can proceed athermally, even at very low temperatures. This explains the lower twinning stress of type II twin relative to its value in the conjugate type I twin, as reported for various materials. In addition, it accounts for the extremely low twinning stress value of type II TB in 10M Ni-Mn-Ga measured at temperatures close to absolute zero.

In compound and type I twins, the equilibrium boundary structure does not contain disconnections. Thus, the rate-limiting step for the motion of the entire TB is the thermally activated nucleation of disconnection loops, resulting in an exponential type kinetic relation. We formulate an expression for the activation energy for nucleation of disconnection loops, and use it to obtain an analytical prediction for the magnitude of the twinning stress. We show that the main material properties that control the twinning stress are the shear modulus μ and the twinning shear s, and obtain a dependence that follows $\sigma_{TS} \propto \mu^2 s^3$. This dependence is in excellent agreement with reported twinning stress in several materials, e.g., Ni-Mn-Ga, Cu-Al-Ni, Ni-Ti and BaTiO₃.

9. Acknowledgments

This research was supported by the United States - Israel Binational Science Foundation (BSF), grant No. 2016662, and by the National Science Foundation NSF-DMR, grant No. 1710640.

Commented [e10]: Is this a good place to relate to twinning stress in steels that falls outside the prediction of Fig. 6?

Commented [CU11R10]: Talking about fcc twinning here would over emphasize that aspect. I would just talk about it in section 7.2.

10. List of symbols and abbreviations

Symbol	Description	units
a,c	Unit cell parameters	length
b	Burgers vector	length
db_{mis}	Burgers vector of infinitesimal dislocation that accounts for interface misfit strain	length
$d_{\scriptscriptstyle TB}$	d_{TB} Lattice spacing perpendicular to a TB plane	
$d_{\scriptscriptstyle D}$	Lattice spacing perpendicular to a TD line	length
DL	Disconnection loop	-
e_f	Formation energy of a kink-pair	Energy
$e_{ m int}$	Interaction energy of kinks in a kink-pair	Energy*length
$E_{\it KP}^{\it self}$	Self-energy of a kink-pair	Energy
E_{DL}^{self}	Self-energy of DL	Energy
E_D^{self}	Self-energy of a linear disconnection	Energy
$E_{\it KP}^{\it existing}$	Total energy of an existing kink-pair	Energy
$E_{\scriptscriptstyle DL}^{\scriptscriptstyle existing}$	Total energy of an existing DL	Energy
$E_{elastic}^{coh.disl.}$	Elastic energy of an array of coherency dislocations	Energy/length
$F_{Peierls}$	Peierls interaction force acting on a disconnection in an array	Force/length
F_{PK}	Peach- Koehler interaction force acting on a disconnection in an array	Force/length
g	Driving force	Energy / volume
$g_{\scriptscriptstyle TS}$	Driving force for TB motion associated with the twinning stress	Energy / volume
g_0	Driving force for TB motion associated with the lattice barrier	Energy / volume
h	Step height of a TD	length
k	Boltzmann constant	Energy / Kelvin
K	K Invariant twinning plane	

KP	Kink pair	-
l_{0}	Equilibrium distance between disconnections in an array on a type II TB	length
$q_{\scriptscriptstyle D}$	Line energy of a DL	Energy/length
Q_{KP}	Activation energy for nucleation of a kink- pair	Energy
$Q_{\scriptscriptstyle DL}$	Activation energy for nucleation of a DL	Energy
Q_D	Activation energy for nucleation of a linear disconnection	Energy
r	Radius of a DL	length
r_c	Critical radius of a DL	length
S	Twinning shear	-
T	Temperature	Kelvin
TB	Twin boundary	-
TD	Twinning disconnection	-
$u_{\scriptscriptstyle D}$	Energy per unit length of a TD	Energy/length
u_D^{bar}	Energy barrier associated with TD motion across the Peierls potential	Energy/length
u_D^{gain}	Energy gain associated with TD motion across the Peierls potential	Energy/length
$U_{{\scriptscriptstyle TB}}$	Energy per unit area of a TB associated with its motion	Energy/area
$U_{\it TB}^{\it bar}$	Energy barrier associated with TB motion across the lattice potential	Energy/area
$U_{\it TB}^{\it gain}$	Energy gain associated with TB motion across the lattice potential	Energy/area
$U_{\mathit{TB}}^{\mathit{mech}}$	Mechanical energy of a TB associated with its motion	Energy/area
$U_{\it TB}^{\it elec}$	Electric energy of a TB associated with its motion	Energy/area
$U_{\it TB}^{\it mag}$	Magnetic energy of a TB associated with its motion	Energy/area
$v_{\scriptscriptstyle TB}$	Velocity of a twin boundary	Length / time

x, y, z	Cartesian coordinates	
x_0	Length of depletion layer near the surface due to uniform motion of a disconnections array	Length
$x_{\scriptscriptstyle D}$	Distance from the surface of a nucleated disconnection	Length
\mathcal{Y}_c	Critical length of a KP	Length
Y	Disconnection length	Length
β	Proportionality factor	10 ³ / GPa
$\gamma_{\scriptscriptstyle TB}$	Amplitude of the lattice barrier for TB motion	Energy /area
$\Gamma_{\scriptscriptstyle D}$	Amplitude of Peierls barrier for TD motion	Energy / length
$\mathcal{E}_{_{S}}$	Longitudinal twinning strain	-
\mathcal{E}_0	Coherency strain on a faceted type II TB	-
η	Twinning shear direction	-
μ	Shear modulus	GPa
ν	Poisson ratio	-
ξ	Line direction of a twinning disconnection (TD)	-
π	Pi, mathematical constant	-
$\sigma_{\!\scriptscriptstyle TS}$	Longitudinal twinning stress	MPa

11. References

- [1] J.W. Christian, S. Mahajan, Deformation twinning, Progress in Materials Science. 39 (1995) 1–157. https://doi.org/10.1016/0079-6425(94)00007-7.
- [2] M.A. Meyers, A. Mishra, D.J. Benson, Mechanical properties of nanocrystalline materials, Progress in Materials Science. 51 (2006) 427–556. https://doi.org/10.1016/j.pmatsci.2005.08.003.
- [3] Y.T. Zhu, X.Z. Liao, X.L. Wu, Deformation twinning in nanocrystalline materials, Progress in Materials Science. 57 (2012) 1–62. https://doi.org/10.1016/j.pmatsci.2011.05.001.
- [4] R.J. Asaro, P. Krysl, B. Kad, Deformation mechanism transitions in nanoscale fcc metals, Philosophical Magazine Letters. 83 (2003) 733–743. https://doi.org/10.1080/09500830310001614540.
- [5] K. Bhattacharya, Microstructure of Martensite: Why it Forms and how it Gives Rise to the Shapememory Effect, OUP Oxford, 2003. http://books.google.co.il/books?id=gas0P67KijcC.

- [6] E. Burcsu, G. Ravichandran, K. Bhattacharya, Large electrostrictive actuation of barium titanate single crystals, Journal of the Mechanics and Physics of Solids. 52 (2004) 823–846. https://doi.org/10.1016/j.jmps.2003.08.001.
- [7] M. Kohl, B. Krevet, S.R. Yeduru, Y. Ezer, A. Sozinov, A novel foil actuator using the magnetic shape memory effect, Smart Materials and Structures. 20 (2011) 094009.
- I. Suorsa, E. Pagounis, K. Ullakko, Position dependent inductance based on magnetic shape memory materials, Sensors and Actuators A: Physical. 121 (2005) 136–141. https://doi.org/10.1016/j.sna.2005.01.001.
- [9] I. Karaman, B. Basaran, H.E. Karaca, A.I. Karsilayan, Y.I. Chumlyakov, Energy harvesting using martensite variant reorientation mechanism in a NiMnGa magnetic shape memory alloy, Applied Physics Letters. 90 (2007). http://dx.doi.org/10.1063/1.2721143.
- [10] E. Bronstein, E. Faran, D. Shilo, Analysis of austenite-martensite phase boundary and twinned microstructure in shape memory alloys: The role of twinning disconnections, Acta Materialia. 164 (2019) 520–529. https://doi.org/10.1016/j.actamat.2018.11.003.
- [11] P. Müllner, Twinning stress of type I and type II deformation twins, Acta Materialia. 176 (2019) 211–219. https://doi.org/10.1016/j.actamat.2019.07.004.
- [12] B.A. Bilby, A.G. Crocker, A.H. Cottrell, The theory of the crystallography of deformation twinning, Proceedings of the Royal Society of London. Series A. Mathematical and Physical Sciences. 288 (1965) 240–255. https://doi.org/10.1098/rspa.1965.0216.
- [13] M. Bevis, A.G. Crocker, L. Rosenhead, Twinning shears in lattices, Proceedings of the Royal Society of London. Series A. Mathematical and Physical Sciences. 304 (1968) 123–134. https://doi.org/10.1098/rspa.1968.0077.
- [14] M. Bevis, A.G. Crocker, L. Rosenhead, Twinning modes in lattices, Proceedings of the Royal Society of London. A. Mathematical and Physical Sciences. 313 (1969) 509–529. https://doi.org/10.1098/rspa.1969.0208.
- [15] Z. Li, C.M. Foster, X. -H. Dai, X. -Z. Xu, S. -K. Chan, D.J. Lam, Piezoelectrically-induced switching of 90° domains in tetragonal BaTiO3 and PbTiO3 investigated by micro-Raman spectroscopy, Journal of Applied Physics. 71 (1992) 4481–4486. https://doi.org/10.1063/1.350792.
- [16] B. Muntifering, L. Kovarik, N.D. Browning, R.C. Pond, W.B. Knowlton, P. Müllner, Stress-assisted removal of conjugation boundaries in non-modulated Ni–Mn–Ga by coordinated secondary twinning, J Mater Sci. 51 (2016) 457–466. https://doi.org/10.1007/s10853-015-9236-1.
- [17] H. Sehitoglu, I. Karaman, R. Anderson, X. Zhang, K. Gall, H.J. Maier, Y. Chumlyakov, Compressive response of NiTi single crystals, Acta Materialia. 48 (2000) 3311–3326. https://doi.org/10.1016/S1359-6454(00)00153-1.
- [18] L. Straka, O. Heczko, H. Seiner, N. Lanska, J. Drahokoupil, A. Soroka, S. Fähler, H. Hänninen, A. Sozinov, Highly mobile twinned interface in 10 M modulated Ni–Mn–Ga martensite: Analysis beyond the tetragonal approximation of lattice, Acta Materialia. 59 (2011) 7450–7463. https://doi.org/10.1016/j.actamat.2011.09.020.
- [19] V. Novák, P. Šittner, S. Ignacová, T. Černoch, Transformation behavior of prism shaped shape memory alloy single crystals, Materials Science and Engineering: A. 438–440 (2006) 755–762. https://doi.org/10.1016/j.msea.2006.02.192.
- [20] K. Kishida, Y. Takahama, H. Inui, Deformation twinning in single crystals of a D019 compound with an off-stoichiometric composition (Ti–36.5at.%Al), Acta Materialia. 52 (2004) 4941–4952. https://doi.org/10.1016/j.actamat.2004.06.051.
- [21] P. Czaja, R. Chulist, K. Nalepka, T. Tokarski, Y.I. Chumlyakov, W. Maziarz, Temperature dependence of twinning stress in Ni49.5Mn38.4Sn12.2 single crystal, Journal of Applied Physics. 126 (2019) 145107. https://doi.org/10.1063/1.5097372.

- [22] A. Sozinov, N. Lanska, A. Soroka, L. Straka, Highly mobile type II twin boundary in Ni-Mn-Ga five-layered martensite, Applied Physics Letters. 99 (2011) 124103–3.
- [23] E. Faran, D. Shilo, Dynamics of twin boundaries in ferromagnetic shape memory alloys, Materials Science and Technology. 30 (2014) 1545–1558. https://doi.org/10.1179/1743284714Y.0000000570.
- [24] O. Heczko, J. Kopeček, L. Straka, H. Seiner, Differently mobile twin boundaries and magnetic shape memory effect in 10M martensite of Ni–Mn–Ga, Materials Research Bulletin. 48 (2013) 5105– 5109. https://doi.org/10.1016/j.materresbull.2013.04.034.
- [25] H. Seiner, L. Straka, O. Heczko, A microstructural model of motion of macro-twin interfaces in Ni– Mn–Ga 10 M martensite, Journal of the Mechanics and Physics of Solids. 64 (2014) 198–211. https://doi.org/10.1016/j.jmps.2013.11.004.
- [26] O. Heczko, L. Straka, H. Seiner, Different microstructures of mobile twin boundaries in 10 M modulated Ni–Mn–Ga martensite, Acta Materialia. 61 (2013) 622–631. https://doi.org/10.1016/j.actamat.2012.10.007.
- [27] L. Straka, N. Lanska, K. Ullakko, A. Sozinov, Twin microstructure dependent mechanical response in Ni--Mn--Ga single crystals, Applied Physics Letters. 96 (2010) 131903.
- [28] S. Kaufmann, R. Niemann, T. Thersleff, U.K. Rößler, O. Heczko, J. Buschbeck, B. Holzapfel, L. Schultz, S. Fähler, Modulated martensite: why it forms and why it deforms easily, New J. Phys. 13 (2011) 053029. https://doi.org/10.1088/1367-2630/13/5/053029.
- [29] L. Straka, J. Drahokoupil, O. Pacherová, K. Fabiánová, V. Kopecký, H. Seiner, H. Hänninen, O. Heczko, The relation between lattice parameters and very low twinning stress in Ni50Mn25\$\mathplus\$xGa25-xmagnetic shape memory alloys, Smart Mater. Struct. 25 (2015) 025001. https://doi.org/10.1088/0964-1726/25/2/025001.
- [30] O. Heczko, V. Kopecký, A. Sozinov, L. Straka, Magnetic shape memory effect at 1.7 K, Applied Physics Letters. 103 (2013) 072405. https://doi.org/10.1063/1.4817941.
- [31] M. Vronka, H. Seiner, O. Heczko, Temperature dependence of twinning stress Analogy between Cu–Ni–Al and Ni–Mn–Ga shape memory single crystals, Philosophical Magazine. 97 (2017) 1479–1497. https://doi.org/10.1080/14786435.2017.1303577.
- [32] L. Straka, A. Soroka, H. Seiner, H. Hänninen, A. Sozinov, Temperature dependence of twinning stress of Type I and Type II twins in 10M modulated Ni–Mn–Ga martensite, Scripta Materialia. 67 (2012) 25–28. https://doi.org/10.1016/j.scriptamat.2012.03.012.
- [33] A. Soroka, A. Sozinov, N. Lanska, M. Rameš, L. Straka, K. Ullakko, Composition and temperature dependence of twinning stress in non-modulated martensite of Ni-Mn-Ga-Co-Cu magnetic shape memory alloys, Scripta Materialia. 144 (2018) 52–55. https://doi.org/10.1016/j.scriptamat.2017.09.046.
- [34] O. Heczko, L. Straka, Temperature dependence and temperature limits of magnetic shape memory effect, Journal of Applied Physics. 94 (2003) 7139–7143. https://doi.org/10.1063/1.1626800.
- [35] J.P. Hirth, Dislocations, steps and disconnections at interfaces, Journal of Physics and Chemistry of Solids. 55 (1994) 985–989. http://dx.doi.org/10.1016/0022-3697(94)90118-X.
- [36] J.P. Hirth, R.C. Pond, Steps, dislocations and disconnections as interface defects relating to structure and phase transformations, Acta Materialia. 44 (1996) 4749–4763. https://doi.org/10.1016/S1359-6454(96)00132-2.
- [37] R.C. Pond, J.P. Hirth, Defects at Surfaces and Interfaces, in: H. EHRENREICH, D. TURNBULL (Eds.), Academic Press, 1994: pp. 287–365. http://www.sciencedirect.com/science/article/pii/S0081194708606414.
- [38] R.C. Pond, X. Ma, Y.W. Chai, J.P. Hirth, Chapter 74 Topological Modelling of Martensitic Transformations, in: F.R.N. Nabarro, J.P. Hirth (Eds.), Elsevier, 2007: pp. 225–261. https://doi.org/10.1016/S1572-4859(07)80006-4.

- [39] R.C. Pond, S. Celotto, Special interfaces: military transformations, International Materials Reviews. 48 (2003) 225–245. https://doi.org/10.1179/095066003225010245.
- [40] R.C. Pond, J.P. Hirth, Topological model of type II deformation twinning, Acta Materialia. 151 (2018) 229–242. https://doi.org/10.1016/j.actamat.2018.03.014.
- [41] R.C. Pond, J.P. Hirth, K.M. Knowles, Topological model of type II deformation twinning in NiTi martensite, Philosophical Magazine. 99 (2019) 1619–1632. https://doi.org/10.1080/14786435.2019.1587185.
- [42] B. Karki, P. Müllner, R. Pond, Topological model of type II deformation twinning in 10M Ni-Mn-Ga, Acta Materialia. 201 (2020) 604–616. https://doi.org/10.1016/j.actamat.2020.10.020.
- [43] J.P. Hirth, J. Wang, Extension of the classical theory for types I and II twinning, Journal of Materials Research. (2021). https://doi.org/10.1557/s43578-020-00003-6.
- [44] A.S.K. Mohammed, H. Sehitoglu, Modeling the interface structure of type II twin boundary in B19' NiTi from an atomistic and topological standpoint, Acta Materialia. 183 (2020) 93–109. https://doi.org/10.1016/j.actamat.2019.10.048.
- [45] H. Seiner, Two-dimensional laminates in monoclinic-II modulated martensites, International Journal of Solids and Structures. 221 (2021) 92–102. https://doi.org/10.1016/j.ijsolstr.2020.04.016.
- [46] E. Faran, D. Shilo, The kinetic relation for twin wall motion in NiMnGa, Journal of the Mechanics and Physics of Solids. 59 (2011) 975–987. https://doi.org/10.1016/j.jmps.2011.02.009.
- [47] E. Faran, D. Shilo, The kinetic relation for twin wall motion in NiMnGa—part 2, Journal of the Mechanics and Physics of Solids. 61 (2013) 726–741. https://doi.org/10.1016/j.jmps.2012.11.004.
- [48] A. Saren, D. Musiienko, A.R. Smith, K. Ullakko, Pulsed magnetic field-induced single twin boundary motion in Ni–Mn–Ga 5M martensite: A laser vibrometry characterization, Scripta Materialia. 113 (2016) 154–157. http://dx.doi.org/10.1016/j.scriptamat.2015.10.020.
- [49] A. Saren, T. Nicholls, J. Tellinen, K. Ullakko, Direct observation of fast-moving twin boundaries in magnetic shape memory alloy Ni–Mn–Ga 5 M martensite, Scripta Materialia. 123 (2016) 9–12. http://dx.doi.org/10.1016/j.scriptamat.2016.04.004.
- [50] R. Abeyaratne, J.K. Knowles, On the driving traction acting on a surface of strain discontinuity in a continuum, Journal of the Mechanics and Physics of Solids. 38 (1990) 345–360. https://doi.org/10.1016/0022-5096(90)90003-M.
- [51] R. Abeyaratne, J.K. Knowles, Evolution of Phase Transitions: A Continuum Theory, Cambridge University Press, 2006. http://books.google.co.il/books?id=GFh4N8rWfS0C.
- [52] D.A. Porter, K.E. Easterling, Phase Transformations in Metals and Alloys, Third Edition (Revised Reprint), Taylor & Francis, 1992. https://books.google.co.il/books?id=eYR5Re5tZisC.
- [53] P. Müllner, K. Ullakko, The Force of a Magnetic/Electric Field on a Twinning Dislocation, Physica Status Solidi (b). 208 (1998) R1–R2. https://doi.org/10.1002/(SICI)1521-3951(199807)208:1<R1::AID-PSSB99991>3.0.CO;2-4.
- [54] P. Müllner, V.A. Chernenko, M. Wollgarten, G. Kostorz, Large cyclic deformation of a Ni-Mn-Ga shape memory alloy induced by magnetic fields, Journal of Applied Physics. 92 (2002) 6708–6713. https://doi.org/10.1063/1.1513875.
- [55] E. Faran, I. Benichou, S. Givli, D. Shilo, The effects of magnetic and mechanical microstructures on the twinning stress in Ni-Mn-Ga, Journal of Applied Physics. 118 (2015) 244104. https://doi.org/10.1063/1.4939179.
- [56] L. Truskinovsky, A. Vainchtein, Kinetics of Martensitic Phase Transitions: Lattice model, SIAM Journal on Applied Mathematics. 66 (2005) 533–553. https://doi.org/10.1137/040616942.
- [57] J.D. Clayton, A continuum description of nonlinear elasticity, slip and twinning, with application to sapphire, Proceedings of the Royal Society A: Mathematical, Physical and Engineering Science. 465 (2009) 307–334. https://doi.org/10.1098/rspa.2008.0281.

- [58] S.R. Kalidindi, Incorporation of deformation twinning in crystal plasticity models, Journal of the Mechanics and Physics of Solids. 46 (1998) 267–290. https://doi.org/10.1016/S0022-5096(97)00051-3.
- [59] E. Faran, D. Shilo, Ferromagnetic Shape Memory Alloys—Challenges, Applications, and Experimental Characterization, Experimental Techniques. 40 (2016) 1005–1031. https://doi.org/10.1007/s40799-016-0098-5.
- [60] P. Müllner, V.A. Chernenko, G. Kostorz, Stress-induced twin rearrangement resulting in change of magnetization in a Ni–Mn–Ga ferromagnetic martensite, Scripta Materialia. 49 (2003) 129–133. https://doi.org/10.1016/S1359-6462(03)00219-7.
- [61] A. Sozinov, N. Lanska, A. Soroka, W. Zou, 12% magnetic field-induced strain in Ni-Mn-Ga-based non-modulated martensite, Applied Physics Letters. 102 (2013). https://doi.org/10.1063/1.4775677.
- [62] J.M. Howe, R.C. Pond, J.P. Hirth, The role of disconnections in phase transformations, Prog Mater Sci. 54 (2009) 47–47. https://doi.org/10.1016/j.pmatsci.2009.04.001.
- [63] R.C. Pond, B. Muntifering, P. Müllner, Deformation twinning in Ni2MnGa, Acta Materialia. 60 (2012) 3976–3984. https://doi.org/10.1016/j.actamat.2012.03.045.
- [64] R.C. Pond, J.P. Hirth, A. Serra, D.J. Bacon, Atomic displacements accompanying deformation twinning: shears and shuffles, Materials Research Letters. 4 (2016) 185–190. https://doi.org/10.1080/21663831.2016.1165298.
- [65] M. Nishida, K. Yamauchi, I. Itai, H. Ohgi, A. Chiba, High resolution electron microscopy studies of twin boundary structures in B19' martensite in the Ti-Ni shape memory alloy, Acta Metallurgica et Materialia. 43 (1995) 1229–1234. https://doi.org/10.1016/0956-7151(94)00328-F.
- [66] Y. Liu, Z.L. Xie, Twinning and detwinning of ⟨0 1 1⟩ type II twin in shape memory alloy, Acta Materialia. 51 (2003) 5529–5543. https://doi.org/10.1016/S1359-6454(03)00417-8.
- [67] Z.L. Xie *, Y. Liu, HRTEM study of (011) type II twin in NiTi shape memory alloy, Philosophical Magazine. 84 (2004) 3497–3507. https://doi.org/10.1080/14786430412331283596.
- [68] Y. Liu, Z.L. Xie, The Rational Nature of Type II Twin in NiTi Shape Memory Alloy, Journal of Intelligent Material Systems and Structures. 17 (2006) 1083–1090. https://doi.org/10.1177/1045389X06064887.
- [69] H. Yan, C. Zhang, Y. Zhang, X. Wang, C. Esling, X. Zhao, L. Zuo, Crystallographic insights into Ni-Co-Mn-In metamagnetic shape memory alloys, Journal of Applied Crystallography. 49 (2016) 1585– 1592. https://doi.org/10.1107/S1600576716012140.
- [70] J. Wang, H. Sehitoglu, Twinning stress in shape memory alloys: Theory and experiments, Acta Materialia. 61 (2013) 6790–6801. https://doi.org/10.1016/j.actamat.2013.07.053.
- [71] K.M. Knowles, A high-resolution electron microscope study of nickel-titanium martensite, Philosophical Magazine A. 45 (1982) 357–370. https://doi.org/10.1080/01418618208236176.
- [72] J.P. Hirth, J. Lothe, Theory of Dislocations, 2nd Edition (Reprint Edition 1992), Krieger Publishing Company, 1982. http://books.google.co.il/books?id=LFZGAAAAYAAJ.
- [73] X. Ding, T. Lookman, Z. Zhao, A. Saxena, J. Sun, E.K.H. Salje, Dynamically strained ferroelastics: Statistical behavior in elastic and plastic regimes, Physical Review B. 87 (3) 094109.
- [74] M. Boleininger, M. Gallauer, S.L. Dudarev, T.D. Swinburne, D.R. Mason, D. Perez, Statistical mechanics of kinks on a gliding screw dislocation, Phys. Rev. Research. 2 (2020) 043254. https://doi.org/10.1103/PhysRevResearch.2.043254.
- [75] A.S.K. Mohammed, H. Sehitoglu, Strain-sensitive topological evolution of twin interfaces, Acta Materialia. 208 (2021) 116716. https://doi.org/10.1016/j.actamat.2021.116716.
- [76] J.P. Hirth, R.W. Armstrong, Straight and curved disclinations and dislocation equivalents, Philosophical Magazine. 0 (2020) 1–13. https://doi.org/10.1080/14786435.2020.1809730.

- [77] G.B. Olson, M. Cohen, Interphase-boundary dislocations and the concept of coherency, Acta Metallurgica. 27 (1979) 1907–1918. https://doi.org/10.1016/0001-6160(79)90081-6.
- [78] A.P. Sutton, R.W. Balluffi, Interfaces in crystalline materials, Clarendon Press, 1995. https://books.google.co.il/books?id=oKLvAAAAMAAJ.
- [79] A.E. Romanov, W. Pompe, J.S. Speck, Theory of microstructure and mechanics of the ...a1/a2/a1/a2... domain pattern in epitaxial ferroelectric and ferroelastic films, Journal of Applied Physics. 79 (1996) 4037–4049. https://doi.org/10.1063/1.361866.
- [80] N. Farag, M. Bobeth, W. Pompe, A.E. Romanov, J.S. Speck, Modeling of twinning in epitaxial (001)-oriented La0.67Sr0.33MnO3 thin films, Journal of Applied Physics. 97 (2005) 113516. https://doi.org/10.1063/1.1914950.
- [81] H.H. Johnson, Strain Energy of Screw Dislocation Arrays, Journal of Applied Physics. 37 (1966) 1763–1766. https://doi.org/10.1063/1.1708598.
- [82] M. Reinhold, D. Kiener, W.B. Knowlton, G. Dehm, P. Müllner, Deformation twinning in Ni–Mn–Ga micropillars with 10M martensite, Journal of Applied Physics. 106 (2009) 053906. https://doi.org/10.1063/1.3211327.
- [83] D. Musiienko, A. Saren, L. Straka, M. Vronka, J. Kopeček, O. Heczko, A. Sozinov, K. Ullakko, Ultrafast actuation of Ni-Mn-Ga micropillars by pulsed magnetic field, Scripta Materialia. 162 (2019) 482– 485. https://doi.org/10.1016/j.scriptamat.2018.12.009.
- [84] L. Dai, J. Cullen, M. Wuttig, Intermartensitic transformation in a NiMnGa alloy, Journal of Applied Physics. 95 (2004) 6957–6959. http://dx.doi.org/10.1063/1.1687203.
- [85] J. Wang, H. Sehitoglu, Martensite modulus dilemma in monoclinic NiTi-theory and experiments, International Journal of Plasticity. 61 (2014) 17–31. https://doi.org/10.1016/j.ijplas.2014.05.005.
- [86] P. Šesták, M. Černý, J. Pokluda, Elastic Constants of Austenitic and Martensitic Phases of NiTi Shape Memory Alloy, in: T. Brezina, R. Jablonski (Eds.), Recent Advances in Mechatronics, Springer Berlin Heidelberg, Berlin, Heidelberg, 2010: pp. 1–6. https://doi.org/10.1007/978-3-642-05022-0_1.
- [87] G. Ren, H. Sehitoglu, Interatomic potential for the NiTi alloy and its application, Computational Materials Science. 123 (2016) 19–25. https://doi.org/10.1016/j.commatsci.2016.06.012.
- [88] E. Faran, D. Shilo, Implications of twinning kinetics on the frequency response in NiMnGa actuators, Applied Physics Letters. 100 (2012) 151901–4.
- [89] A. Saren, K. Ullakko, Dynamic twinning stress and viscous-like damping of twin boundary motion in magnetic shape memory alloy Ni-Mn-Ga, Scripta Materialia. 139 (2017) 126–129. https://doi.org/10.1016/j.scriptamat.2017.06.010.
- [90] B. Karki, Y. Behar, I. Harel, E. Caplan, A. Sabbag, D. Shilo, P. Mullner, E. Faran, A simple method to characterize high rate twin boundary kinetics in Ni-Mn-Ga, Review of Scientific Instruments. 90 (2019) 105107. https://doi.org/10.1063/1.5109934.
- [91] A. Mizrahi, U. Heller, E. Faran, D. Shilo, Under-microscope Mechanical Pulse System for Studying Deformation Processes at High Strain Rates, Experimental Mechanics. 60 (2020) 191–204. https://doi.org/10.1007/s11340-019-00555-7.
- [92] A. Mizrahi, D. Shilo, E. Faran, Variability of Twin Boundary Velocities in 10M Ni–Mn–Ga Measured Under μs-Scale Force Pulses, Shap. Mem. Superelasticity. (2020). https://doi.org/10.1007/s40830-020-00264-4
- [93] M. Avrami, Kinetics of Phase Change. I General Theory, The Journal of Chemical Physics. 7 (1939) 1103–1112. https://doi.org/10.1063/1.1750380.
- [94] M. Avrami, Kinetics of Phase Change. II Transformation-Time Relations for Random Distribution of Nuclei, The Journal of Chemical Physics. 8 (1940) 212–224. https://doi.org/10.1063/1.1750631.
- [95] R. Abeyaratne, C. Chu, R.D. James, Kinetics of materials with wiggly energies: Theory and application to the evolution of twinning microstructures in a Cu-Al-Ni shape memory alloy, Philosophical Magazine A. 73 (1996) 457–497. https://doi.org/10.1080/01418619608244394.

- [96] R.B. Flippen, Domain wall dynamics in ferroelectric/ferroelastic molybdates, Journal of Applied Physics. 46 (1975) 1068–1071. https://doi.org/10.1063/1.322212.
- [97] N. Zreihan, E. Faran, D. Shilo, The effect of loading rate on characteristics of type II twin boundary motion in Ni-Mn-Ga, Scripta Materialia. 144 (2018) 44–47. https://doi.org/10.1016/j.scriptamat.2017.09.045.
- [98] T. Ezaz, H. Sehitoglu, Type II detwinning in NiTi, Appl. Phys. Lett. 98 (2011) 141906. https://doi.org/10.1063/1.3574775.
- [99] H. Sehitoglu, J. Jun, X. Zhang, I. Karaman, Y. Chumlyakov, H.J. Maier, K. Gall, Shape memory and pseudoelastic behavior of 51.5%Ni–Ti single crystals in solutionized and overaged state, Acta Materialia. 49 (2001) 3609–3620. https://doi.org/10.1016/S1359-6454(01)00216-6.
- [100] L. Straka, A. Sozinov, J. Drahokoupil, V. Kopecký, H. Hänninen, O. Heczko, Effect of intermartensite transformation on twinning stress in Ni-Mn-Ga 10 M martensite, Journal of Applied Physics. 114 (2013) 063504. https://doi.org/10.1063/1.4817717.
- [101] A. Sozinov, A. Soroka, N. Lanska, M. Rameš, L. Straka, K. Ullakko, Temperature dependence of twinning and magnetic stresses in Ni46Mn24Ga22Co4Cu4 alloy with giant 12% magnetic fieldinduced strain, Scripta Materialia. 131 (2017) 33–36. https://doi.org/10.1016/j.scriptamat.2016.12.032.
- [102] T.E. Stenger, J. Trivisonno, Ultrasonic study of the two-step martensitic phase transformation in \${\mathrm{Ni}}_{2}\mathrm{MnGa}\$, Phys. Rev. B. 57 (1998) 2735–2739. https://doi.org/10.1103/PhysRevB.57.2735.
- [103] M. Stipcich, L. Mañosa, A. Planes, M. Morin, J. Zarestky, T. Lograsso, C. Stassis, Elastic constants of \$\mathrm{Ni}\text{\ensuremath{-}}\mathrm{Ga}\$ magnetic shape memory alloys, Phys. Rev. B. 70 (2004) 054115. https://doi.org/10.1103/PhysRevB.70.054115.
- [104] Q. Hu, C.-M. Li, R. Yang, S. Kulkova, D.I. Bazhanov, B. Johansson, L. Vitos, Site occupancy, magnetic moments, and elastic constants of off-stoichiometric Ni2MnGa from first-principles calculations, (2009). https://doi.org/10.1103/PHYSREVB.79.144112.
- [105] N. Glavatska, G. Mogylny, I. Glavatskiy, V. Gavriljuk, Temperature stability of martensite and magnetic field induced strain in Ni–Mn–Ga, Scripta Materialia. 46 (2002) 605–610.
- [106] N. Zreihan, E. Faran, D. Shilo, The effects of temperature on the lattice barrier for twin wall motion, Applied Physics Letters. 107 (2015) 041605. https://doi.org/10.1063/1.4927660.
- [107] Z. Li, The elastic and electromechanical properties of tetragonal BaTiO3 single crystals, (n.d.) 7.
- [108] N. Lanska, O. Söderberg, A. Sozinov, Y. Ge, K. Ullakko, V.K. Lindroos, Composition and temperature dependence of the crystal structure of Ni–Mn–Ga alloys, Journal of Applied Physics. 95 (2004) 8074–8078. https://doi.org/10.1063/1.1748860.
- [109] N. Otani, Y. Funatsu, S. Ichinose, S. Miyazaki, K. Otsuka, Orientation dependence of the deformation modes in a γl' martensite single crystal in CuAlNi alloy, Scripta Metallurgica. 17 (1983) 745–750. https://doi.org/10.1016/0036-9748(83)90486-6.
- [110] O. Söderberg, L. Straka, V. Novák, O. Heczko, S.-P. Hannula, V.K. Lindroos, Tensile/compressive behaviour of non-layered tetragonal Ni52.8Mn25.7Ga21.5 alloy, Materials Science and Engineering: A. 386 (2004) 27–33. https://doi.org/10.1016/j.msea.2004.07.045.
- [111] B. Reinholz, S. Brinckmann, A. Hartmaier, B. Muntifering, W.B. Knowlton, P. Müllner, Influence of the twin microstructure on the mechanical properties in magnetic shape memory alloys, Acta Materialia. 108 (2016) 197–206. http://dx.doi.org/10.1016/j.actamat.2016.02.007.